PERSPECTIVE

Check for updates

Spin-flip methods in quantum chemistry

David Casanova [ID] *[ab] and Anna I. Krylov [ID] [c]

This Perspective discusses salient features of the spin-flip approach to strong correlation and describes different methods that sprung from this idea. The spin-flip treatment exploits the different physics of low-spin and high-spin states and is based on the observation that correlation is small for same-spin electrons. By using a well-behaved high-spin state as a reference, one can access problematic low-spin states by deploying the same formal tools as in the excited-state treatments (*i.e.,* linear response, propagator, or equation-of-motion theories). The Perspective reviews applications of this strategy within wave function and density functional theory frameworks as well as the extensions for molecular properties and spectroscopy. The utility of spin-flip methods is illustrated by examples. Limitations and proposed future directions are also discussed.

1 Introduction

Quantum chemistry is the cornerstone of theoretical modeling of molecules and materials. The complexity and variability of

[a] *Donostia International Physics Center (DIPC), 20018 Donostia, Euskadi, Spain.*
 E-mail: david.casanova@ehu.eus
[b] *IKERBASQUE, Basque Foundation for Science, 48013 Bilbao, Euskadi, Spain*
[c] *Department of Chemistry, University of Southern California, Los Angeles,*
 California 90089, USA

molecular electronic structure makes this field both exciting and challenging. *Ab initio* electronic structure theory[1] aims to solve the time-independent electronic Schrödinger equation, whose solutions provide electronic wave functions and potential energy surfaces governing nuclear motions. Wave functions are objects of intimidating complexity: they depend explicitly on $3n$ coordinates of n electrons and parametrically on the nuclear positions. The recipe for obtaining the exact (non-relativistic) solution is deceptively simple – one just needs to solve a variational problem for the full configuration interaction (FCI) ansatz.

David Casanova is an Ikerbasque Research Associate at the Donostia International Physics Center (DICP). Casanova's research focuses on the development and implementation of electronic structure for excited states and strongly correlated systems. Casanova is also using these methods to study optoelectronic and magnetic properties of molecular materials and to investigate underlying photophysical processes. Casanova holds a master degree in Chemistry (U Girona) and in Physics

David Casanova

(U Barcelona). After his PhD studies in Chemistry, he joined Prof. Head-Gordon's group at the UC Berkeley as a Fulbright Research Fellow. In 2009 he received a Ramón y Cajal Fellowship (U Complutense Madrid and U Barcelona) and in 2013 he became an Ikerbasque Research Fellow at the U Basque Country. Since 2018 Casanova is Associate Professor at the DIPC.

Anna Krylov is the Gabilan Distinguished Professor in Science and Engineering and a Professor of Chemistry at the University of Southern California. Krylov develops theoretical models for open-shell and electronically excited species, including metastable states. Using computational chemistry, Krylov investigates the role of radicals and electronically excited species in combustion, solar energy, bioimaging, and quantum information science. Krylov has received

Anna I. Krylov

the Dirac Medal (WATOC), the Theoretical Chemistry Award (ACS/PHYS), Bessel Research Award (Humboldt Foundation), Mildred Dresselhaus Award (DESY and Hamburg Univ.), and Plyler Prize for Molecular Spectroscopy & Dynamics (APS). She is a Fellow of the ACS, APS, and AAAS; an elected member of the Int'l Academy of Quantum Molecular Science; a Board Member of WATOC; and a 2018 Simons Foundation Fellow in Theoretical Physics.

However, owing to the factorial scaling of the FCI configurational space, this brute-force strategy remains applicable only to rather small molecules (up to 20 electrons), in spite of great strides in the development of efficient algorithms[2–7] and progress in computer architectures. Hence, practical quantum chemistry is build upon systematic approximations to the exact solution. Within wave function theory, the hierarchy of approximations begins with the Hartree–Fock (HF) model, in which electrons interact only *via* the mean field and are, therefore, uncorrelated. Then, gradual improvements in the description of explicit electron–electron interactions are made by incremental improvements in treating electron correlation.

Electron correlations can be loosely divided into two types: (i) a few large contributions arising from (near-)degenerate configurations (static or non-dynamic correlation) and (ii) numerous small contributions arising from many excited configurations (dynamic correlation). Hence, proper treatment of static correlation requires the use of multi-configurational wave functions in which several leading configurations can be described on an equal footing. Although, traditionally, multi-configurational ansätze have been equated with multi-reference approaches,[8,9] the two are not the same. While the word 'multi-configurational' reflects the physics of the problem, the adjective 'multi-reference' describes a particular formalism of attaining a multi-configurational ansatz. In the multi-reference approaches one constructs a zero-order wave function by a system- and state-dependent selection of important configurations meant to capture the non-dynamic correlation, which is subsequently augmented by configurations needed to describe dynamic correlation. In this perspective, we describe a family of methods following an alternative strategy, *i.e.*, obtaining multi-configurational wave functions within a single-reference formalism.

A classic example of strong correlation (*i.e.*, a situation characterized by large non-dynamic correlation) is a molecule with stretched bonds: when bonding and anti-bonding orbitals become close in energy, at least two configurations are necessary to describe the ground-state wave function. Fig. 1 shows potential energy curves for the ground and lowest triplet states of H_2. Around the equilibrium geometry, a single determinant $(\sigma)^2$ captures the main features of the exact ground state wave function, and the difference between HF and FCI is dominated by dynamic correlation. At larger interatomic separations, the σ and σ^* orbitals become closer in energy and the exact wave function acquires a two-configurational character. Consequently, the quality of the HF approximation plummets at the dissociation limit, *i.e.*, the correlation energy becomes huge, exceeding the dissociation energy by several electron-volts. On the other hand, the $\alpha\alpha$ component of the triplet state $^3[(\sigma)^1(\sigma^*)^1]$ is not affected by orbital degeneracies and retains single-determinantal character at all internuclear separations.

This different behavior of the low- and high-spin states, such as S_0 and T_1 ($M_S = 1$), in the presence of degeneracies (or near-degeneracies) of the frontier molecular orbitals, along with the observation that all important low-spin configurations are formally single excitations from the high-spin reference, inspired the strategy of building strongly correlated wave functions from a
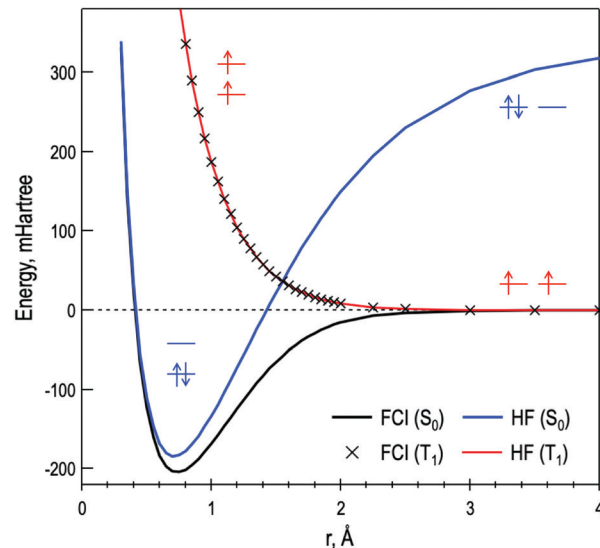

Fig. 1 HF and FCI energy curves of the ground state singlet (S_0) and the $M_S = 1$ component of the triplet (T_1) states of H_2 along bond-breaking coordinate; STO-3G basis.

well-behaved high-spin reference determinant.[10] Specifically, the multi-configurational low-spin states can be accessed by single excitations that flip the spin of one of the spin-up (α) electrons. Thus, spin-flip ansätze are generated by the action of a spin-flipping excitation operator on a single high-spin reference determinant. This approach is capable of tackling a broad class of strongly correlated problems while retaining the theoretical elegance and black-box nature of single-reference approaches.[11] By combining the spin-flip idea with different models for electron correlation, one arrives at a hierarchy of methods, ranging from low-level inexpensive models to highly accurate methods systematically converging to FCI.

The earliest use of spin-flip transformations can be traced back to Bethe, who applied them to construct antiferromagnetic states of cyclic spin chains from a ferromagnetic spin configuration.[12] Later, spin-flip excitation operators were explicitly defined by Shibuya and McKoy[13] and applied to quantum-chemistry problems.[14,15] Despite this early scattered usage of spin-flipping excitations, the formal theory of spin-flip methods in molecular electronic structure was established only in 2001 by Krylov in the framework of the equation-of-motion coupled-cluster (EOM-CC)[16] and configuration interaction (CI)[17] formalisms. Since then, various flavors of spin-flip methods have been developed within wave function theory[18–30] and density functional theory (DFT).[31–35] Recently, a spin-flip version of simplified TD-DFT aiming at very large molecules has been reported.[36] Spin-flip methods have been successfully applied to study bond-breaking,[37] diradicals,[38–48] triradicals,[49–56] polyradicals,[57–59] crossings of potential energy surfaces and conical intersections,[60–71] magnetic couplings in single-molecule magnets,[72–77] singlet fission phenomena,[78–83] non-linear optical properties,[84,85] and excited-state processes.[86,87]

This perspective provides an overview of spin-flip methods and their applications. We revisit the theory and describe the attributes of different spin-flip approaches, highlighting

their strengths, deficiencies, and limitations through illustrative examples. This work does not provide an exhaustive review of all efforts in this area; rather, it aims to complement several excellent reviews.[10,88,89]

2 Spin-flip wave function theory

Several theoretical frameworks have been used for developing quantum-chemical models for treating excited states: response theory,[90] equation-of-motion (EOM)[91,92] and electron propagator techniques (Green's function).[93] In the EOM formalism, one obtains energy differences by explicitly separating the reference and target states through the use of excitation operators. In single-reference formalisms, the choice of the reference determinant defines the separation between the occupied and virtual orbital spaces and the excitation operators are defined as operators containing only creation operations in the virtual space (particles, or p) and annihilation operators in the occupied space (holes, or h). For example, excited states can be accessed by $1h1p$ excitation operators acting on a closed-shell determinant representing the ground state.

The EOM reference state is not meant to provide a zero-order description of a particular target state; rather, it serves as a convenient device for generating balanced configurational expansion.[94] This framework facilitates the generalization of EOM to excitation operators that do not conserve the number of electrons, such as in the EOM-IP/EA (ionization potential/ electron attachment) variants, or that do not conserve spin projection (M_S), such as in spin-flip methods. Different flavors of EOM methods are illustrated in Fig. 2. A similar strategy of separating the reference states and using excitation operators to access different manifolds of target states is exploited within algebraic diagrammatic construction (ADC) approaches.[95] Collectively, these methods, formulated using hole-particle operators, are known as Fock-space methods, and different manifolds of target states constitute different sectors in the Fock space.

In the coupled-cluster framework,[96] target EOM-CC states are obtained by solving an eigenproblem for a non-Hermitian Hamiltonian:

$$\bar{\hat{H}}\hat{R}^k|\Phi_0\rangle = \omega_k \hat{R}^k|\Phi_0\rangle, \qquad (1)$$

where $|\Phi_0\rangle$ is the reference Slater determinant, $\hat{R}^k$ is an excitation operator connecting $|\Phi_0\rangle$ with the k-th target state $|\Psi^k\rangle = \hat{R}^k|\Phi_0\rangle$, $\bar{\hat{H}} \equiv e^{-\hat{T}} H e^{\hat{T}}$ is the similarity-transformed Hamiltonian, $\hat{T}$ is the cluster excitation operator computed for the reference state, and ω_k is the excitation energy relative to the reference state. In practice, eqn (1) is approximated by truncating the excitation level in $\hat{T}$ and $\hat{R}$ (typically, at the same excitation level), e.g., in EOM-EE-CCSD $\hat{T} \approx \hat{T}_1 + \hat{T}_2$ and $\hat{R} \approx \hat{R}_0 + \hat{R}_1 + \hat{R}_2$.

In contrast to EOM-EE-CC, in which the EOM operators are particle and spin conserving (i.e., have the same number of α and β creation and annihilation operators and are, therefore, of the $M_S = 0$ type), the spin-flip variant of EOM-CC (EOM-SF-CC)[16,19] is defined by an excitation operator ($\hat{R}^{SF} \equiv \hat{R}(M_S = -1)$)
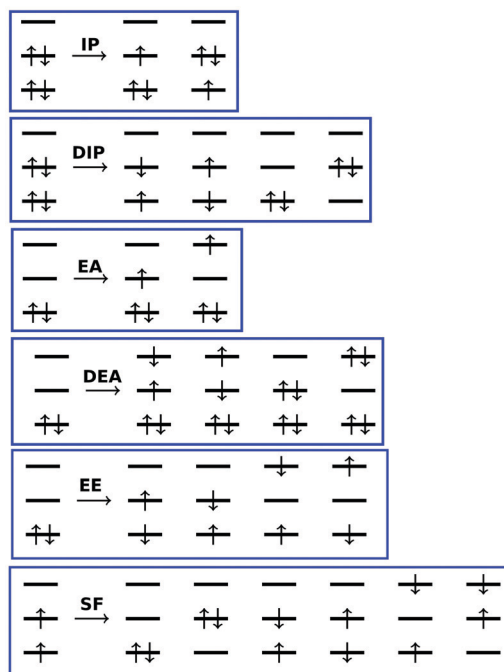

Fig. 2 In the EOM formalism, different manifolds of target states are described by combining a particular reference state and a particular type of excitation operators. For example, electronically excited states are described by particle- and spin-conserving excitations from (usually) a closed-shell reference corresponding to the ground state, giving rise to the EOM-EE method. Cationic or neutral doublet states can be described by ionizing operators (i.e., $1h$, $2h1p$, etc.) acting on a closed-shell reference, giving rise to EOM-IP. Doubly ionizing operators ($2h$, $3h1p$) can be used to access diradical-type or doubly ionized states (EOM-DIP). In a similar fashion, electron attaching operators ($1p$, $2p1h$) acting on a closed-shell reference provide access to anionic or neutral doublet states (EOM-EA). Double electron attaching operators ($2p$, $3p1h$) provide access to diradical states or to a subset of excited states derived from excitation from HOMO (EOM-DEA). By using high-spin references and spin-flipping operators, other types of multi-configurational states can be described (EOM-SF, EOM-DSF). Using excitation operators in a similar fashion, ADC family of methods is built upon perturbation theory and propagator formalisms.

expanded in terms of excitation operators including a spin-flip of one electron ($\alpha \to \beta$), i.e., operators of the $M_S = -1$ type:

$$\hat{R}_1^{SF} = \sum_{ia} r_i^a a_\beta^\dagger i_\alpha, \qquad (2)$$

$$\hat{R}_2^{SF} = \frac{1}{2}\sum_{ijab} r_{ij}^{ab} a_\beta^\dagger i_\alpha b_\sigma^\dagger j_\sigma, \dots \qquad (3)$$

where the i, j and a, b indices run over occupied and virtual orbitals (as defined by $|\Phi_0\rangle$), $a_\sigma^\dagger$ (i_σ) is a creation (annihilation) operator of an electron in the a_σ (i_σ) spin-orbital ($\sigma = \alpha, \beta$), and the state index k is omitted for brevity.

When $\hat{R}^{SF}$ acts on the reference state, it generates a set of determinants with $\Delta M_S = -1$ with respect to $|\Phi_0\rangle$. For example, for an $M_S = 1$ triplet reference, it yields a set of the $M_S = 0$ configurations, which can be used to describe low-spin target singlet and triplet states, whereas for an $M_S = 3/2$ quartet

4328 | *Phys. Chem. Chem. Phys.*, 2020, **22**, 4326–4342

This journal is © the Owner Societies 2020

reference, it yields a set of the $M_S = 1/2$ configurations, which can be used to describe doublet and quartet states.

In addition to EOM-SF-CCSD, the spin-flip operator has been combined with other many-body models, such as the optimized orbitals CCD (SF-OO-CCD or SF-OD for short),[97] EOM-MP2,[27] and the ADC scheme.[29] As in the standard many-body treatments of the excited states, the accuracy can be systematically improved by explicit or perturbative account of triple excitations, as, for example, in the EOM-SF-CCSD(dT) and EOM-SF-CCSD(fT) methods[20] where (dT) and (fT) are two alternative choices to introduce non-iterative triples corrections to EOM-CCSD. Spin-flip methods within the CI framework (SF-CI)[17,18] can be derived from the EOM-SF-CC eigen-problem (eqn (1)) by setting $\hat{T} = 0$. Importantly, SF-CI treatments are both variational and size-extensive.[17,21,98] Several ways of generating spin-flip configurational space have been explored, giving rise to different flavors of SF-CI models.[17,18,21,22,24,30,98]

2.1 EOM-EE versus EOM-SF strategy: benzynes example

Benzynes are prototypical aromatic diradicals with tunable diradical character derived by removing two hydrogen atoms from benzene. Fig. 3 shows frontier natural orbitals of ortho-, meta-, and para-benzyne. As the distance between the carbons formally hosting the unpaired electrons increases from the ortho- to meta- and para-species, so does the extent of the diradical character. In all three benzynes, the ground state is singlet and the gap between the singlet and the lowest triplet can serve as a measure of the diradical character.[52] The latter can also be quantified by the populations of the natural frontier orbitals of the singlet state[46] (for the triplet states, natural frontier orbitals have populations close to one). As one can see from Fig. 3, the difference in populations of the two natural orbitals in ortho-benzyne is quite substantial, revealing predominantly closed-shell character. In contrast, in para-benzyne, in which the two radical centers are further apart, the populations
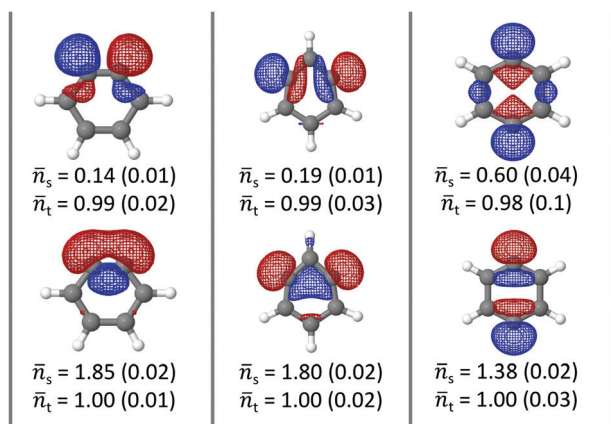
Table 1 Adiabatic singlet–triplet gaps (eV) in benzynes (positive gap corresponds to the singlet being below the triplet)

Method[a]	$o\text{-}C_6H_4$	$m\text{-}C_6H_4$	$p\text{-}C_6H_4$
ΔCCSD	1.343	0.510	−0.771
EOM-EE-CCSD	1.477	0.655	−0.578
EOM-SF-CCSD[b]	1.578	0.782	0.147
EOM-SF-CCSD(fT)[b]	1.615	0.875	0.169
Exp.[c]	1.656	0.868	0.144

[a] cc-pVTZ basis, core electrons frozen, geometries from ref. 38. [b] From ref. 20. [c] Electronic energies, experimental[99,100] adiabatic energies corrected by ZPE, see ref. 34.

become closer. The increased diradical character in the ortho → meta → para series manifests itself in the shrinking singlet–triplet gap.[20,34,38,99,100]

Table 1 shows the experimental and theoretical singlet–triplet gaps (adiabatic electronic energies) in ortho-, meta-, and para-benzyne. The theoretical values are computed at the same equilibrium geometries[38] so that the differences between the methods can be clearly assessed. As one can see, computing the energy gap as the difference between the total CCSD energies of the lowest singlet and lowest triplet state (ΔCCSD) systematically underestimates the gap because the energy of the triplet is too low. This is a numeric illustration of the correlation being smaller in the high-spin states than in the low-spin states.[16] In ortho-benzyne, in which the singlet state has small diradical character, the error is not very large, however, it increases in meta- and para-benzyne, to the extent that in para-benzyne, ΔCCSD reverses the state ordering. The situation is slightly improved when the triplet state is described by EOM-EE-CCSD from the closed-shell singlet reference because of the more-balanced nature of this approach, however, the triplet still appears too low relative to the singlet. In the spin-flip calculations, the singlets and triplets are described on an equal footing, resulting in much better agreement with the experimental gaps even at the CCSD level; the inclusion of triples further improves the results.

2.2 Performance of various spin-flip models for a perfect diradical: cyclobutadiene

Cyclobutadiene is a popular benchmark system, in which the energy gap between the frontier orbitals and, consequently, the diradical character, can be tuned by varying nuclear positions: at square (D_{4h}) structures the two frontier orbitals are exactly degenerate by symmetry, whereas symmetry lowering to D_{2h} lifts the degeneracy. Due to the second-order Jahn–Teller effect, the equilibrium ground state structure is rectangular (D_{2h}), with alternating double and single bonds. At this structure, the two frontier orbitals are well separated in energy and the X^1A_g state has only very weak multi-configurational character. Hence, the ground and low-lying excited states can be well described by single-reference methods. The equilibrium geometry of the triplet state is D_{4h}. Interestingly, the triplet state (1^3A_{2g}), in which the two e_g frontier orbitals are singly occupied,

Fig. 3 Frontier natural orbitals and their occupations of the lowest singlet and triplet (low-spin) states of ortho-, meta-, and para-benzynes. $\bar{n} = |n_\alpha + n_\beta|$, with $\Delta n = |n_\alpha − n_\beta|$ provided in parentheses. $\bar{n}_s$ and $\bar{n}_t$ correspond to $\bar{n}$ values obtained from the occupancies of the singlet and triplet natural orbitals, respectively. The values are computed using the EOM-SF-CCSD/cc-pVTZ wave functions. Reproduced with permission from ref. 46.

This journal is © the Owner Societies 2020

Phys. Chem. Chem. Phys., 2020, **22**, 4326–4342 | **4329**

is above the singlet state even at the triplet state equilibrium geometry, thus violating Hund's rule. The lowest singlet (X^1B_{1g}) has two-configurational character and can be described as a perfect singlet diradical. This is a typical case of a strongly correlated system, where standard (non-spin-flip) single-reference methods for the ground and excited states, such as HF/CIS or CCSD/EOM-EE-CCSD, are completely unreliable; whereas, spin-flip methods easily capture the main features of the four lowest electronic states.

Fig. 4a shows ground-state total energies computed with a variety of spin-flip models. Already the lowest-level spin-flip model, SF-CIS, is able to recover the strong correlation in X^1B_{1g} arising due to the equal contributions of the two configurations with one of the two e_g orbitals being doubly occupied. However, the lack of dynamic correlation manifests itself in a much higher total energy relative to highly correlated methods such as EOM-SF-CCSD(dT/fT).[20] Interestingly, the effect of triples is small and EOM-SF-CCSD total energy is very close to that of EOM-SF-CCSD(dT/fT). In contrast to EOM-SF-CCSD, SF-CISD
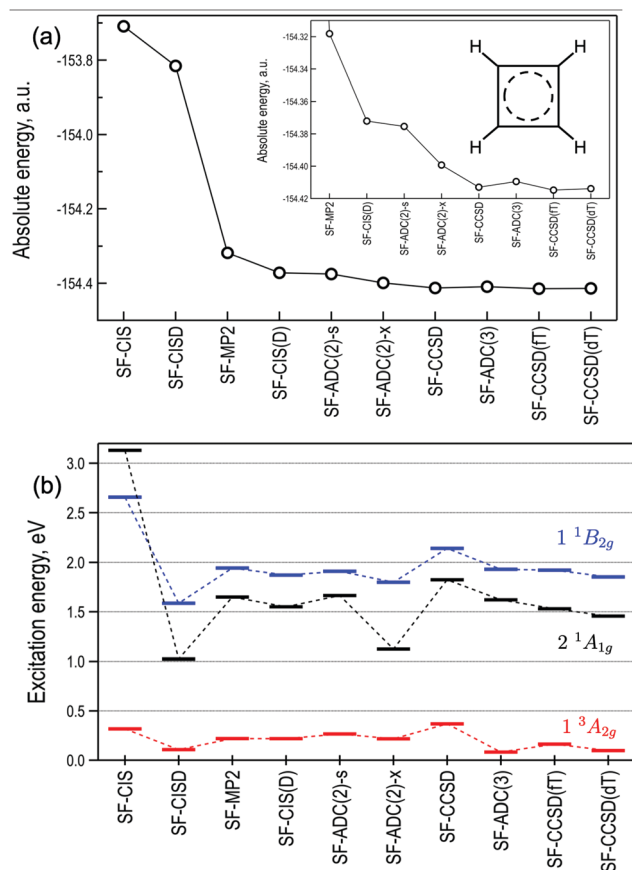

(a)

(b)

Fig. 4 Spin-flip description of the ground and excited states of cyclobutadiene within CC, CI, and ADC frameworks. Panel (a): total energies (Hartree) of the ground state (X^1B_{1g}). Panel (b): vertical excitation energies (eV) for the low-lying states, 1^3A_{2g} (red), 1^1B_{2g} (blue), and 2^1A_{1g} (black) at the 1^3A_{2g} square planar optimized geometry of cyclobutadiene.[19] The calculations used the cc-pVTZ basis and UHF triplet reference. Core electrons frozen in EOM-SF-MP2 and EOM-SF-CCSD calculations. 'EOM' label was omitted to reduce clutter. SF-ADC(2)-s, SF-ADC(2)-x and SF-ADC(3) values are from ref. 29. SF-CCSD(dT)/(fT) values are from ref. 20.

only mildly improves upon the SF-CIS energy, showing that explicit doubles within the linear spin-flip ansatz capture only a small fraction of the electron–electron instantaneous interactions. On the other hand, SF-CIS(D) accounts for a much larger fraction of the electron correlation, yielding total energy much closer to EOM-SF-CCSD(dT/fT), because SF-CIS(D) corresponds to a perturbative approximation to EOM-SF-CCSD and contains the $\hat{U}_1^{SF}\hat{T}_2$ term not present in SF-CISD:

$$E^{SF\text{-}CIS(D)} = \langle \Psi^{SF\text{-}CIS} | \hat{V} | \hat{U}_2^{SF} \Phi^{(0)} \rangle + \langle \Psi^{SF\text{-}CIS} | \hat{V} | \hat{U}_1^{SF} \hat{T}_2 \Phi^{(0)} \rangle \quad (4)$$

where $\hat{V}$ is the fluctuation potential, and $\hat{U}_1^{SF}$, $\hat{U}_2^{SF}$, and $\hat{T}_2$ are excitation operators defined by perturbation theory[18] – their form is the same as that of the EOM-CC operators.

The approximation of the T-amplitudes at the MP2 level[101] (EOM-SF-MP2) and the strict second-order ADC (SF-ADC(2)-s) energies are very close to the SF-CIS(D) result, while the extended variant (SF-ADC(2)-x) underestimates the energy of 2^1A_{1g} (the couplings between doubly excited configurations, which are not contained in the SF-ADC(2)-s matrix, are included in an *ad hoc* fashion in SF-ADC(2)-x). The third order ADC scheme (SF-ADC(3)) systematically improves total energies towards EOM-SF-CCSD and EOM-SF-CCSD(dT/fT).

As illustrated by Fig. 4b, all spin-flip methods yield very similar singlet–triplet gaps, close to the reference EOM-SF-CCSD(dT/fT) values of 0.10–0.16 eV. The excitation energies of the singlet states appear to be more sensitive to dynamical correlation and show more variation. SF-CIS swaps the ordering of the 1^1B_{2g} and 2^1A_{1g} states. The correct ordering is restored upon inclusion of double excitations. Double excitations are particularly important for the 2^1A_{1g} state, as indicated by the weight of the $\hat{R}_2^{SF}$ terms: 7.4% (4.1%) (X^1B_{1g}), 6.8% (5.7%) (1^3A_{2g}), 13.2% (9.4%) (2^1A_{1g}), and 8.1% (6.7%) (1^1B_{2g}) at the SF-CISD (EOM-SF-CCSD) level. Overall, SF-CIS(D), SF-ADC(n), and EOM-SF-CCSD yield rather similar excitation energies for the singlet excited states. We note that the inclusion of perturbative triples in EOM-SF-CCSD systematically redshifts the transition energies by ~ 0.3 eV.

3 Spin-flip time-dependent density functional theory

3.1 Linear response TDDFT

Within the DFT framework, excited states are typically described through linear-response (LR) TDDFT. In LR-TDDFT, excitation energies and excited-state properties can be obtained from Casida's equation,

$$\begin{bmatrix} \mathbf{A} & \mathbf{B} \\ \mathbf{B}^* & \mathbf{A}^* \end{bmatrix} \begin{bmatrix} \mathbf{X} \\ \mathbf{Y} \end{bmatrix} = \omega \begin{bmatrix} \mathbf{1} & \mathbf{0} \\ \mathbf{0} & -\mathbf{1} \end{bmatrix} \begin{bmatrix} \mathbf{X} \\ \mathbf{Y} \end{bmatrix}, \quad (5)$$

where ω is the excitation energy, the $\mathbf{X}$ and $\mathbf{Y}$ vectors contain transition amplitudes, and the elements of the $\mathbf{A}$ and $\mathbf{B}$ matrices are:

$$A_{ia,jb} = \delta_{ij}\delta_{ab}(\varepsilon_a - \varepsilon_i) + \frac{\partial F_{ia}}{\partial P_{jb}}, \quad B_{ia,jb} = \frac{\partial F_{ia}}{\partial P_{bj}}, \quad (6)$$

4330 | *Phys. Chem. Chem. Phys.*, 2020, **22**, 4326–4342

This journal is © the Owner Societies 2020

where ε_p is the energy associated with the Kohn–Sham (KS) orbital ϕ_p. Eqn (5) is usually solved considering the adiabatic approximation (AA), *i.e.*, assuming instantaneous electronic transition upon infinitesimal perturbation, resulting in frequency-independent exchange-correlation (xc) kernels and loss of memory. The matrix terms coupling electronic excitations in the **A** and **B** blocks (eqn (5)) correspond to the Fock matrix (**F**) derivatives with respect to the density matrix (**P**), which for non-hybrid functionals and spin-conserving (collinear) time-dependent perturbations can be expressed as:

$$\frac{\partial F_{pq}}{\partial P_{st}} = (pq|f_{\mathrm{H}}|st) + (pq|f_{\mathrm{xc}}|st), \qquad (7)$$

where f_{H} and f_{xc} are the Hartree and xc kernels, and the two-electron integrals are given in Mulliken's notation:

$$(pq|f_{\mathrm{H}}|st) = \int \phi_p{}^*(\mathbf{x})\phi_q(\mathbf{x})\frac{1}{|\mathbf{r} - \mathbf{r}'|}\phi_t{}^*(\mathbf{x}')\phi_s(\mathbf{x}')\mathrm{d}\mathbf{x}\mathrm{d}\mathbf{x}', \qquad (8)$$

$$(pq|f_{\mathrm{xc}}|st) = \int \phi_p{}^*(\mathbf{x})\phi_q(\mathbf{x})\frac{\delta^2 E_{\mathrm{xc}}}{\delta\rho(\mathbf{r})\delta\rho(\mathbf{r}')}\phi_t{}^*(\mathbf{x}')\phi_s(\mathbf{x}')\mathrm{d}\mathbf{x}\mathrm{d}\mathbf{x}', \qquad (9)$$

with $\mathbf{x} = (\mathbf{r},\sigma)$ and $\sigma = \alpha, \beta$. For general hybrid xc functionals, eqn (7) can be written as:

$$\frac{\partial F_{pq}}{\partial P_{st}} = (pq|f_{\mathrm{H}}|st) + (1 - c_{\mathrm{HF}})(pq|f_{\mathrm{xc}}|st) - c_{\mathrm{HF}}(ps|f_{\mathrm{H}}|qt), \qquad (10)$$

where c_{HF} determines the amount of exact exchange.

Although DFT and TDDFT can, in principle, deliver exact answers whether the underlying wave functions are multi-configurational or not, their current implementations within the KS and LR/AA frameworks inherit the limitations of single-reference methods. In other words, KS-DFT works well for systems whose wave function description is dominated by a single Slater determinant. Furthermore, because LR-TDDFT with AA admits only single-electron excitations, it is blind to the existence of doubly excited states. Consequently, standard KS-DFT and LR-TDDFT fail for the strongly correlated systems in exactly the same way as single-reference wave function methods. Likewise, the spin-flip approach to multi-configurational wave functions works well within the KS-TDDFT framework. Just as in the wave-function based methods, one can describe problematic cases with (near-)degenerate frontier MOs by using a high-spin KS reference determinant and treating the target manifold of the low-spin states as spin-flipped TDDFT states.

Benchmark studies illustrated robust performance of SF-TDDFT for a variety of strongly correlated systems, ranging from organic diradicals[31,34,43] to single-molecule magnets[72–74,77] and conical intersections.[35,71,86] Just as in the case of standard DFT, the results depend on the functional employed, but consistently reliable results (often, with an accuracy comparable to wave function methods) can be obtained using rationally chosen functionals.

It is worth mentioning that SF-TDDFT is not free from the problems stemming from self-interaction errors present in pure density functionals. For example, SF-TDDFT does not improve upon regular TDDFT in the description of electronic transitions with small hole/electron overlaps, such as charge-transfer excitations or Rydberg states. Just as in spin-conserved TDDFT, these situations call for hybrid functionals with substantial Hartree–Fock exchange, especially for large inter-electron separations, as in the long-range corrected functionals.

3.2 Collinear SF-TDDFT

In the case of $\alpha \rightarrow \beta$ spin non-conserving transitions, *i.e.*, considering the $\alpha\beta$ and $\beta\alpha$ blocks of the **X** and **Y** amplitudes, only interactions that originate from the exact exchange survive spin-symmetry requirements, and the spin-flip $\alpha\beta$, $\alpha\beta$ and $\alpha\beta$, $\beta\alpha$ terms of the **A** and **B** coupling matrices for a hybrid functional simplify to:

$$A_{i\bar{a},j\bar{b}} = \delta_{ij}\delta_{\bar{a}\bar{b}}(\varepsilon_{\bar{a}} - \varepsilon_i) - c_{\mathrm{HF}}(ij|f_{\mathrm{H}}|\bar{a}\bar{b}); \quad B_{i\bar{a},\bar{j}b} = -c_{\mathrm{HF}}(ib|f_{\mathrm{H}}|\bar{a}\bar{j}), \qquad (11)$$

where the upper bars indicate β spin-orbitals. Hence, the energy spectrum computed with pure xc functionals ($c_{\mathrm{HF}} = 0$) corresponds to energy differences of the non-interacting single-electron states (*i.e.*, Koopmans' picture). The need to mix the exact exchange into the xc functional in order to capture state interaction effects was pointed out by Shao and coworkers in their original SF-TDDFT paper.[31] The best performance resulting from the direct application of the spin-flip excitation operator to LR-TDDFT is achieved with functionals containing about 50% HF exchange, such as BHHLYP, 50-50, or PBE50.[34,77] Interestingly, the increase of the exact exchange allows one to recover the degeneracy between spin-multiplet components.[33,102]

3.3 The effect of exact exchange in SF-TDDFT: excited states in Be

To illustrate the importance of the exact exchange in SF-TDDFT, let us consider the electronic spectrum of the Be atom. The ground state of beryllium corresponds to the $1s^2 2s^2$ configuration and the low-lying excited states are derived by single and double $2s \rightarrow 2p$ excitations, giving rise to $1s^2 2s^1 2p^1$ and $1s^2 2p^2$ states. The standard (non-spin-flip) TDDFT cannot access the latter states because they lack double excitations, but SF-TDDFT from the high-spin triplet reference of $(1s)^2(2s)^1(2p)^1$ character can. Fig. 5 shows SF-TDDFT/TDA/6-31G energies computed using the $^3P(M_S = 1)$ reference with BLYP (0% HF exchange), B3LYP (20% HF exchange), and BHHLYP (50% HF exchange) functionals compared to the FCI energies.

The excitation energies computed with the pure GGA functional are rather inaccurate, but systematically improve with increasing amount of HF exchange (Fig. 5). The two lowest excited states of Be correspond to the (triply degenerate) triplet (^3P) and singlet (^1P) states, both with the $1s^2 2s^1 2p^1$ electronic configuration. At the SF-BLYP level, ^1P and ^3P appear as degenerate, as their energies are simply given by the $2s/2p$ energy gap (eqn (11)). Configuration interaction through the exact exchange breaks the $^3P/^1P$ degeneracy and notably improves the energy of both states, specially ^1P, which blueshifts from 3.21 eV (BLYP) to 4.92 eV (BHHLYP). The higher ^1D and the second ^3P states are double excitations with respect to the ground state ($1s^2 2s^2 \rightarrow 1s^2 2p^2$), and cannot be recovered by spin-conserving TDDFT within the AA. On the other hand,
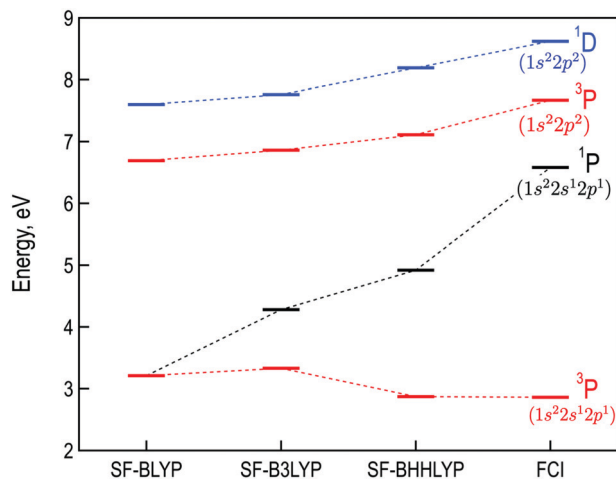
This journal is © the Owner Societies 2020

Phys. Chem. Chem. Phys., 2020, **22**, 4326–4342 | **4331**

Fig. 5 Low-lying electronic states of Be computed with FCI and SF-TDDFT with GGA functionals with different amounts of the exact exchange: 0% (BLYP), 20% (B3LYP), and 50% (BHHLYP), and the 6-31G basis set.

SF-TDDFT can describe these transitions, although spin contamination for the highest ^3P state is large (see Section 5).

3.4 Non-collinear SF-TDDFT

The use of non-relativistic (collinear) xc kernels precludes using SF-TDDFT within the domain of pure density functionals as it relies on the Hartree–Fock exchange potential to couple spin-flip excitations. To circumvent this limitation, Ziegler et al. considered non-collinear functionals in SF-TDDFT,[32,103,104] in the same fashion as in relativistic DFT.[105,106] In the absence of spin–orbit coupling and taking single-particle eigenstates of $\hat{S}_z$, i.e., α or β spin-orbitals, the collinear and non-collinear potentials are identical, but they respond differently to the action of a time-dependent perturbation. Specifically, while the first order change in $\rho_{\alpha\beta}$ only induces the second order change of the collinear xc potential, it can cause a linear response in the non-collinear xc potential resulting in a spin-flip excitation with αβ, αβ coupling terms given as:

$$\frac{\partial F_{p\bar{q}}}{\partial P_{s\bar{t}}} = \int \phi_p(\mathbf{r})\phi_{\bar{q}}(\mathbf{r})\frac{1}{\rho_\alpha - \rho_\beta}\left(\frac{\delta E_{xc}}{\delta\rho_\alpha} - \frac{\delta E_{xc}}{\delta\rho_\beta}\right)\phi_s(\mathbf{r})\phi_{\bar{t}}(\mathbf{r})d\mathbf{r}. \quad (12)$$

Consequently, the non-collinear representation of the xc functional[107–109] naturally mixes the high-spin KS reference configuration with the $M_S = 0$ states through the changes in the $\rho_{\alpha\beta}$ density.

The generalization of SF-TDDFT with non-collinear GGA and hybrid kernels was first developed and implemented within TDA by Rinkevicius and collaborators,[43,110] and later extended to full SF-TDDFT response by Li and Liu.[111] Li and Liu also noted that TDA is better suited for spin-flip applications than RPA, since the latter might suffer from the reference instabilities. Benchmarking studies have confirmed the improvement of the SF-TDDFT performance with non-collinear kernel for the xc functionals with moderate amounts of exact exchange ($<50\%$) in the characterization of electronic structure of diradical and

triradical species.[34,77] While in most cases (various organic diradicals, single-molecule magnets), the performance of collinear SF-TDDFT with B5050LYP was on par with that of non-collinear SF-TDDFT with the best-performing functionals, one notable exception is same-center diradicals, such as open-shell atoms and carbenes. Singlet–triplet energy gaps in these systems are rather inaccurate when computed with collinear SF-TDDFT (see Fig. 5), but systematically improve with non-collinear SF-TDDFT using the functionals belonging to the PBE family (in particular PBE50). It has been shown that the origin of this problem arises from an overestimation of the $M_S = 0$ triplet energy.

An important flaw of non-collinear GGA is the unphysical behavior when $\rho_\alpha(\mathbf{r}) \approx \rho_\beta(\mathbf{r})$ while the α- and β-density gradients remain different at the same point $\mathbf{r}$ (see eqn (12)). Such numerical instabilities can be mitigated by the use of tight grids in energy calculations, but remain problematic in gradient calculations. A simple and computationally effective solution to circumvent numerical instabilities in non-collinear GGA kernels is to set $\nabla\rho_\alpha = \nabla\rho_\beta = 0$, which was named as the ALDA0 approximation.[111]

3.5 Collinear versus non-collinear SF-TDDFT: TMM diradical

Trimethylenemethane (TMM) is the simplest non-Kekulé diradical. It has four π-electrons giving rise to the triplet ground state[41,112–114] with two unpaired electrons in the doubly degenerate e' frontier orbitals (Fig. 6a). The ground-state structure of TMM belongs to the D_{3h} symmetry. The low-lying states are derived from different distributions of the four π-electrons in the four orbitals.

Here we analyze the performance of collinear and non-collinear SF-TDDFT for vertical excitation energies to the twofold degenerate $^1E''$ singlet and $^3E'$ triplet, and the $^1A_1'$ state of TMM at the D_{3h} ground-state minimum. The accuracy of SF-TDDFT energies is evaluated with respect to the EOM-SF-OD values from Slipchenko and Krylov.[38] As Fig. 6b shows, SF-TDDFT generally underestimates transition energies to $^1E''$, $^1A_1'$, and $^3E'$, with improved values for larger HF exchange fraction for both collinear and non-collinear kernels, the latter systematically being more accurate. The best excitation energies are obtained with 50% of the exact exchange. Noteworthy, collinear SF-PBE (no exact exchange) fails to recover electronic excitations within the e' set, and $^1E''$ and $^1A_1'$ states are obtained as degenerate with the ground state triplet. On the other hand, the nonzero αβ, αβ coupling matrix elements in the non-collinear form of the functional lift this degeneracy and yield physically meaningful values with pure density functionals.

4 Using spin-flip methods to describe conical intersections and transitions between states of same and different multiplicities

Non-adiabatic transitions between states of the same (internal conversion) or different (intersystem crossing) multiplicity are two major relaxation pathways in excited-state processes.[115–117] By virtue of Fermi's golden rule, the rate of such electronic transitions is proportional to the square of the coupling matrix
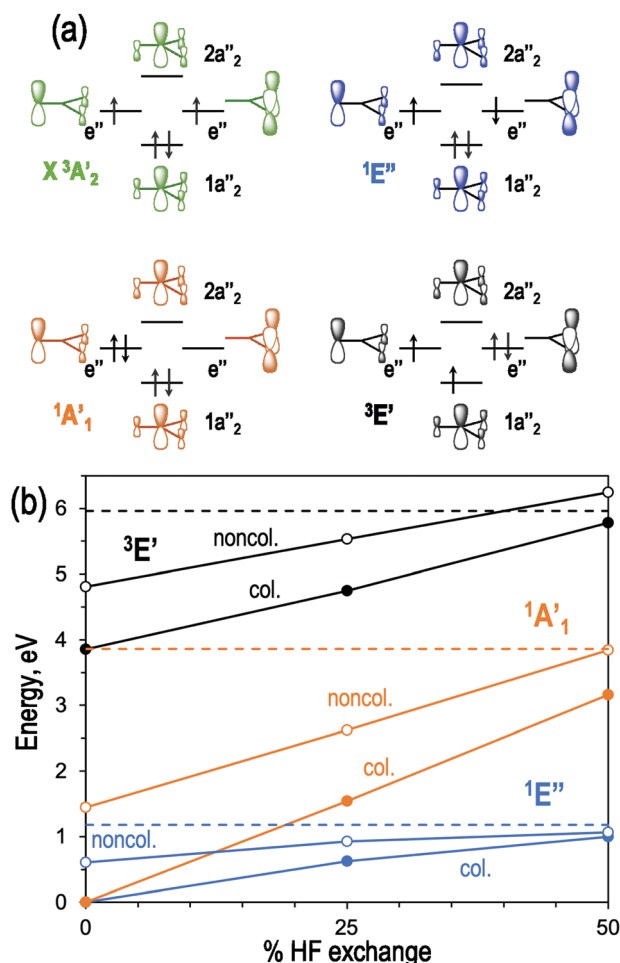
4332 | Phys. Chem. Chem. Phys., 2020, **22**, 4326–4342

This journal is © the Owner Societies 2020

Fig. 6 (a) Molecular orbital diagram for the ground (X^3A_2') and low-lying electronic states $(^1E'', {}^1A_1',$ and $^3E')$ of the TMM diradical. (b) Collinear (full circles) and non-collinear (empty circles) SF-TDDFT/TDA vertical transition energies of TMM computed with the PBE xc functional mixed with different amounts of HF exchange and the cc-pVTZ basis set. Dashed lines indicate the reference values obtained with SF-OD.[38]

element (*i.e.*, non-adiabatic or spin–orbit coupling) and inversely proportional to the energy gap between the states. Thus, the ability to correctly describe electronic degeneracies and to treat multiple interacting states on the same footing are the key prerequisites for modeling radiationless relaxation and spin-forbidden processes.

Both spin-allowed and spin-forbidden non-adiabatic transitions are most effective in regions where two or more states are nearly degenerate. In particular, radiationless relaxation is facilitated by conical intersections (CoIns),[116,118,119] *i.e.*, crossings of potential energy surfaces of states with the same symmetry.

CoIns are paramount examples of electronic degeneracies. To correctly describe CoIns, the method should be able to treat the intersecting states on the same footing, which presents an obvious problem both for single- and multi-reference methods. Single-reference excited-state methods (*e.g.*, CIS, CIS(D), EOM-EE-CCSD, EE-ADC, TDDFT), can, in general, treat CoIns between the excited states, but fail for the intersections between the ground and excited states because the ground state is treated differently than the excited states. In addition, at CoIns between the ground and excited state, the excited state often acquires doubly excited character with respect to the ground state, which poses problems for standard single-reference methods. Within the multi-reference framework, one faces problems due to state-specific treatments, which often violate exact degeneracies. The common solution is state-averaging, which entails certain arbitrariness and creates problems of its own.[65] The spin-flip approach enables treating CoIns between the ground and excited states within a single-reference formalism.[61,120–123]

The challenges in modeling CoIns have been illustrated by Gozem and collaborators.[65,124,125] Using the retinal chromophore as a model system (Fig. 7, top), they have investigated the ability of electronic structure methods to correctly describe the location of the CoIn between the two lowest electronic states at a twisted geometry (near the *cis–trans* isomerization transition state).[65,124,125] The CoIn in this conjugated molecule originates from the crossing of the $\pi \rightarrow \pi^*$ excited diradical state (Ψ_{DIR}) with the ground-state closed-shell charge-transfer state (Ψ_{CT}). This benchmark is a stringent test of quantum mechanical methods because it requires both the ability to treat multi-configurational and degenerate states on an equal footing, where one of the states also has a charge transfer character. As the reference values, Gozem and coworkers used the MR-CISD+Q (multi-reference configuration interaction with single and double excitations and with Davidson's correction) data. The results for selected methods shown in Fig. 7 clearly illustrate the sensitivity of CoIns to the correlation treatment. For example, CASSCF or MR-CISD without Davidson's correction yield significantly different positions. But by using the triplet $^3\pi\pi^*$ reference, EOM-SF can describe both singlet states on an equal footing. EOM-SF-CCSD(dT) yields the position of CoIns almost exactly on top of that of the reference MR-CISD+Q; it also reproduces the overall shapes of the potential energy surfaces well (*e.g.*, the differences in vertical energies gaps at stationary points are less than 1 kcal mol^{-1} and non-parallelity errors are less than 1.4 kcal mol^{-1}).

Standard LR-TDDFT within the AA suffers from the same problems as the single-reference wave function methods: it fails to account for the diradical nature of molecules in the CoIn region and cannot describe the doubly excited character of relevant excited states. Just as within wave function theory, SF-TDDFT overcomes these limitations. The potential utility of SF-TDDFT in describing CoIns was first suggested by Levine *et al.*[120] and was later exploited by many researchers.[61,62,86,87,122,124]

Ethylene is the simplest molecule exhibiting a rotation around a double bond that leads to the π-bond breaking and electronic degeneracies. In particular, it is well known that ethylene undergoes photoinduced *cis–trans* isomerization through a molecular funnel connecting the lowest excited singlet (S_1) and the ground (S_0) states. Multi-configurational calculations[120,126,127] yielded a minimum-energy crossing point with a twisted CC double bond and the pyramidalization of one of the CH_2 groups (PY in Fig. 8). The collinear SF-TDDFT minimum-energy crossing point for the PY structure agrees well with the reported MRCI results.[61,122] In addition to the PY

This journal is © the Owner Societies 2020

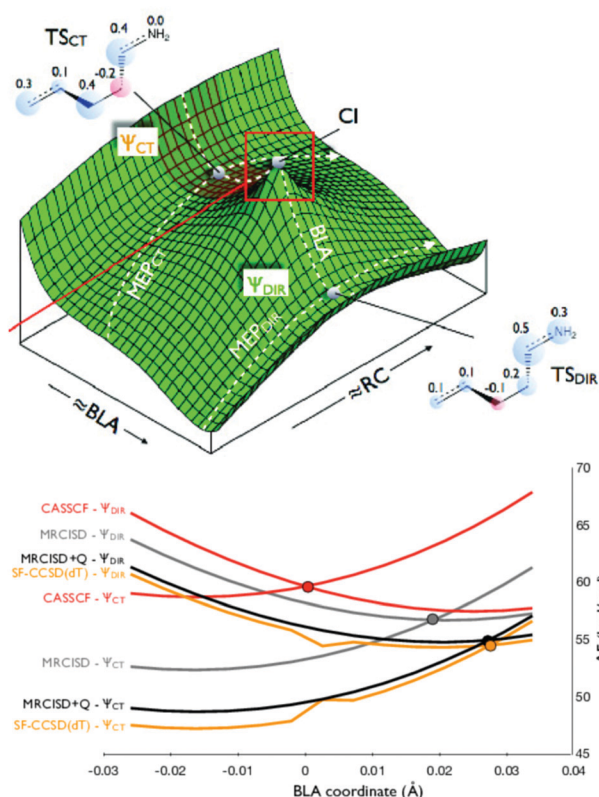*Phys. Chem. Chem. Phys.*, 2020, **22**, 4326–4342 | **4333**

Fig. 7 Top: Potential energy surface in retinal showing the location of the conical intersection (CoIn or CI) between the charge transfer and diradical states. The two coordinates are bond-alternation (BLA) and twisting reaction coordinate (RC). Relevant mechanistic paths are indicated as white dashed lines. MEP_{CT}: minimum energy path on the ground state that connects the *cis* and *trans* retinal equilibrium geometries through a transition state (TS_{CT}). MEP_{DIR}: connects *cis*, TS_{DIR} and *trans* structures of the Ψ_{DIR} state. The BLA path connects the TS_{CT} and TS_{DIR} transition states and also intercepts a CoIn (CI) point. Atomic charges of the two transition states are illustrated by bubble diagrams. Bottom: Potential energy scans along the BLA coordinate using selected methods. Reproduced with permission from ref. 65.

CoIn, other critical points on the S_0/S_1 crossing seam have been investigated in detail, such as the hydrogen-migrated (HM) and ethylidene (ET) structures. While ET is a true (minimum) critical point on the crossing seam, HM is a saddle point.[127] SF-TDDFT is also able to capture the nature of HM and ET crossings. The analysis of the main configurations of the degenerate states at the CoIn indicates the open-shell character of the ground state and the importance of double excitations in the description of these degeneracies.

These results for ethylene (and similar findings by Gozem and coworkers[124] for retinal) demonstrate the suitability of SF-TDDFT for the description of CoIns with accuracy similar to that of highly correlated methods, while preserving the favorable computational cost of TDDFT. Therefore, SF-TDDFT is becoming a workhorse methodology to explore photochemical reactions involving dynamics through the S_0/S_1 CoIns, especially in extended systems and in the condensed phase, where multi-reference approaches are not affordable.[62,63,86] The implementation
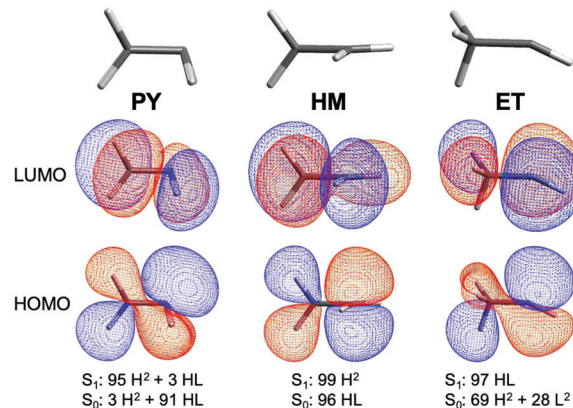

Fig. 8 Optimized geometries (top), reference (T_1) molecular orbitals (middle), and leading configurations in the S_0 and S_1 states (bottom) for the PY, HM and ET minimum-energy crossing points of ethylene computed with SF-BHHLYP/6-31G(d,p).

of SF-TDDFT analytic non-adiabatic couplings[122] opens the door for using this methodology in non-adiabatic dynamics simulations.

Non-adiabatic couplings for other spin-flip methods are also becoming available.[123] In the absence of the full implementation of non-adiabatic couplings, approximate schemes for estimating the couplings from the norm of one-particle transition density matrices were developed[128,129] and employed to estimate the rates of non-adiabatic transitions using RAS-SF wave functions in the context of singlet fission.[80,81,130–132]

Finally, modeling non-adiabatic transitions between electronic states of different multiplicity (intersystem crossing) is now possible[133] due to the implementations of spin–orbit couplings using the Breit–Pauli Hamiltonian and EOM-SF[134,135] wave functions.

5 Spin contamination in spin-flip methods

One of the limitations of many implementations of spin-flip methods relates to spin incompleteness of the spin-flip expansion, which may lead to sizable (artificial) mixing of electronic states with different spin multiplicities. The resulting spin contamination is a common feature in these methods. It originates from the direct use of the spin-flip excitation operator within electronic structure schemes based on the truncation of the excitation operator to a finite *n*-tuple level, such as single excitations in SF-CIS. This problem is largely rectified by expanding the excitation operator to higher-order terms, *e.g.*, from SF-CIS to SF-CISD or SF-CISDT, but at the price of a rapid increase in computational cost. Moreover, there is no simple recipe for going beyond single excitations in the framework of TDDFT within the AA, which creates a conceptual stumbling block in SF-TDDFT.

To properly address spin contamination in spin-flip methods, it is necessary to understand its origin.[136] In the following, we discuss in some detail the two sources of spin contamination of spin-flip states, that is: (i) spin-contaminated reference configuration

and (ii) an incomplete excitation scheme leading to spin incompleteness of the target states.

5.1 Spin-contaminated references

Spin contamination of the reference configuration, *e.g.* $\langle \hat{S}^2 \rangle > 2.0$ for a high-spin triplet, propagates into the target states resulting in spin-flip states with mixed spin character. Spin-impure values in the reference state indicate that the chosen high-spin reference is not well-behaved. This may mean that the chosen reference does not properly reflect all electron-electron strong correlations, in other words, that it does not capture the multi-configurational nature of the system.

Spin-contaminated initial configuration can also result from converging to an undesired state; hence, it is always advisable to verify the nature of the HF or KS reference. Typically, a good high-spin reference state either corresponds to the lowest electronic state in the respective multiplicity or is nearly degenerate with it and is characterized by a small energy gap with the respective low-spin spin-flip state (*e.g.*, the gap between the reference $M_S = 1$ triplet and the target $M_S = 0$ triplet states is a good diagnostic of the quality of the reference state).

The problems due to spin-contaminated reference can often be fixed or improved by using spin-restricted formulations, although ROHF (or ROKS) often leads to convergence difficulties.[137] Other orbital choices rectifying spin contamination include orbitals optimized for a correlated ansatz, such as OO-CCD[138] or OO-MP2,[139,140] or even KS-DFT orbitals.[45,141,142] Using open-shell references can also create problems in schemes involving truncations of the virtual orbital space, such as in frozen natural orbital approaches,[143,144] even when a spin-pure ROHF reference is used; a solution for this problem has been recently reported.[137]

5.1.1 Example: linear H$_4$. Here we use a four-electron system to illustrate the impact of using inappropriate reference configurations in SF-CIS and SF-TDDFT, as manifested by the expectation value of the $\hat{S}^2$ operator. Specifically, we explore the performance of spin-flip methods in calculating the energy gap between the ground-state singlet and the lowest triplet states for the model system of four hydrogen atoms (H$_4$) in a linear arrangement (Fig. 9). First, we consider the case of the two H$_2$ moieties far apart ($D = 7.0$ Å), with one H$_2$ unit being at the equilibrium geometry ($r = 0.743$ Å) and the other with a stretched bond distance ($d = 3.0$ Å). This system has two strongly correlated electrons with a small HOMO-LUMO gap (the frontier orbitals are localized on the stretched H$_2$) and well-separated HOMO−1 and LUMO+1 levels (which are localized on the H$_2$ moiety, which is at the equilibrium geometry). Hence, it can be seen as a system with diradical character; we will refer to it as linear-*D*. Second, we consider four H atoms equally separated at $d = 3.0$ Å. In this situation all four electrons are correlated and the four lowest molecular orbitals lie within a small energy window, much like in a molecular tetraradical (linear-*T*).

In accordance with the near-degeneracy of the frontier orbitals, the two linear forms of H$_4$ exhibit small singlet–triplet gaps (< 0.1 eV), as obtained in the FCI calculations (Table 2). The SF-CIS and SF-TDDFT computed gaps for the linear-*D* H$_4$
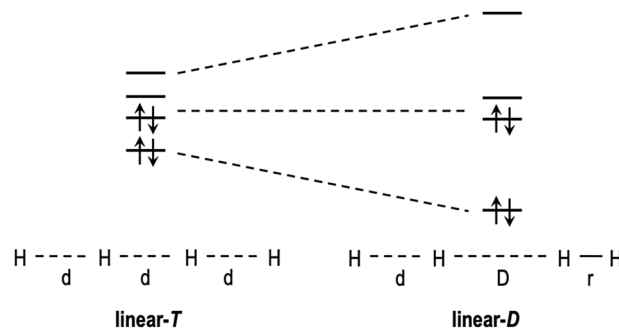

Fig. 9 Molecular orbital diagrams (top) and the structures (bottom) of the model H$_4$ system in two linear arrangements with tetraradical (left: linear-*T*) and diradical (right: linear-*D*) character. Interatomic distances: $d = 3.0$ Å; $D = 7.0$ Å; $r = 0.743$ Å.

Table 2 Relative energies (in eV) of the lowest singlet and triplet states for linear-*D* and linear-*T* structures of H$_4$ computed by FCI, SF-CIS, and collinear SF-PBE50 (TDA) with the 3-21G basis set. $\hat{S}^2$ expectation values are given in parenthesis. $\langle \hat{S}^2 \rangle$ for the reference $M_S = 1$ triplet configuration is shown in italics

State	FCI	SF-CIS	SF-PBE50
Linear-*D*		(*2.000*)	(*2.000*)
S$_0$	0.00	0.00	0.00
	(0.000)	(0.000)	(0.008)
T$_1$	0.04	0.04	0.09
	(2.000)	(2.000)	(1.992)
Linear-*T*		(*2.259*)	(*2.259*)
S$_0$	0.00	0.00	0.00
	(0.000)	(1.273)	(1.020)
T$_1$	0.02	4.66	2.91
	(2.000)	(2.241)	(2.215)

(using the lowest HF/KS triplet as the reference) are in very good agreement with the FCI energy, with $\langle \hat{S}^2 \rangle$ values, perfectly recovering the spin multiplicity of the lowest states. On the other hand, the triplet reference state in the linear-*T* case is not well described by a single Slater determinant ($\langle \hat{S}^2 \rangle > 2.0$). Consequently, the spin-flip computed states show strong spin contamination, and the singlet–triplet energy separation is grossly overestimated.

5.2 Incomplete excitation scheme

The most important source of spin contamination in spin-flip approaches, especially for those effectively restricted to single excitations with respect to the reference configuration, such as SF-CIS and SF-TDDFT, stems from the spin incompleteness of the spin-flip excitation operator applied to a high-spin reference. Similar issues[136] arise in the context of excited-state theories using open-shell references, such as in EOM-EE-CCSD or TDDFT calculations of radicals.[145–147]

To illustrate this problem, here we analyze the spin-flip excitation operator with only one-electron excitations $\left(\hat{R}_1^{\Delta M_S = -1} \right)$. Such an operator, when combined with the HF kernel, defines the SF-CIS method.

When the single spin-flip operator is applied to a high-spin Slater determinant with N_S unpaired spin-α electrons, *e.g.*,
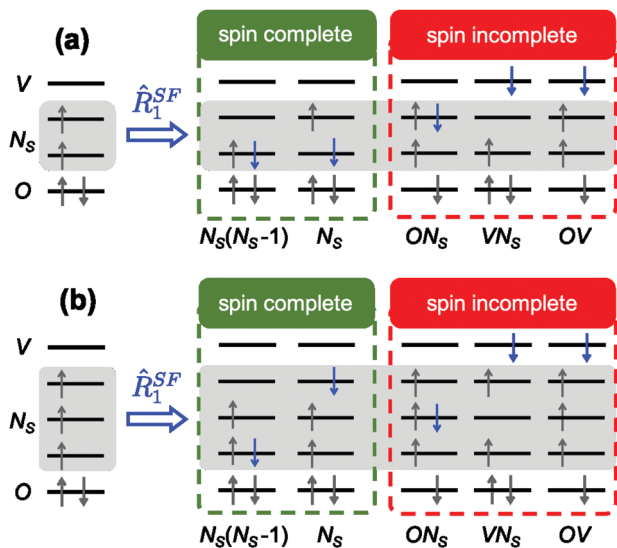
Fig. 10 Representation of the electronic configurations generated by the single spin-flip excitation operator $\left(\hat{R}_1^{SF} \equiv \hat{R}_1^{\Delta M_S = -1}\right)$ acting on the high-spin triplet (a) and quartet (b) configurations. Spin complete and incomplete configurations are framed in green and red, respectively. Spin-flip excited electrons are indicated in blue. N_S, O, and V: singly occupied (highlighted in grey), doubly occupied, and unoccupied virtual orbitals in the reference state. The dimension of each type of configuration subspace is indicated at the bottom.

triplet ($N_S = 2$) or quartet ($N_S = 3$) spin states, it generates a set of configurations that can be classified into different classes (Fig. 10). Such an expansion contains N_S^2 terms resulting from spin-flip excitations within the N_S singly occupied (in the reference) orbitals, comprising $N_S(N_S - 1)$ configurations with $N_S - 1$ unpaired electrons and N_S configurations with N_S unpaired electrons. Each of these two subsets contains all the pieces necessary to form spin-pure wave functions (assuming spin-restricted orbitals). Additionally, the SF-CIS ansatz (and, similarly, SF-TDDFT within AA) includes excitations from the doubly occupied orbital and to virtual orbital spaces, with O and V orbitals, respectively. There are $N_S(O + V)$ configurations with $N_S - 1$ unpaired electrons and OV configurations with $N_S + 2$ unpaired electrons. These sets of configurations are not spin complete, hence, SF-CIS states may not be eigenstates of $\hat{S}^2$, with the extent of spin contamination depending on the weight of the spin-incomplete configurations. States that are primarily described by the configurations from the spin-complete space do not show strong spin state mixing, and should be the ones targeted by spin-flip calculations. However, those states that involve sizable contributions of configurations with a hole (electron) in the doubly occupied (virtual) orbital space suffer from spin incompleteness and would manifest severe spin contamination. The description of these states, typically exhibiting intermediate $\langle \hat{S}^2 \rangle$ values between two spin multiplicities, is not reliable in spin-flip calculations.

5.2.1 Example: methylene diradical. As an example illustrating spin incompleteness, let us consider electronic states of the methylene (CH_2) diradical. Table 3 presents excitation energies

Table 3 Vertical excitation energies (eV) of methylene (CH_2) computed with FCI, SF-CIS, and SF-PBE50 (TDA) with the 6-31G basis set at the CCSD(T)/cc-pVQZ (X^3B_1) optimized geometry.[148] $\hat{S}^2$ expectation values are given in parenthesis

State	FCI	SF-CIS	SF-PBE50
$X\ ^3B_1$	0.00 (2.000)	0.00 (2.044)	0.00 (2.015)
$1\ ^1A_1$	1.50 (0.000)	1.64 (0.019)	0.43 (0.010)
$1\ ^1B_1$	2.09 (0.000)	2.20 (0.029)	1.03 (0.015)
$2\ ^1A_1$	3.76 (0.000)	4.41 (0.050)	2.47 (0.025)
$1\ ^3A_2$	8.31 (2.000)	8.74 (1.025)	6.96 (1.011)
$1\ ^3B_2$	8.78 (2.000)	8.85 (1.008)	7.19 (1.003)
$3\ ^1A_1$	8.85 (0.000)	9.39 (1.017)	7.62 (1.009)
$1\ ^1A_2$	8.98 (0.000)	10.12 (1.106)	8.34 (1.040)
$2\ ^3B_1$	9.31 (2.000)	11.51 (1.013)	9.44 (1.006)
$1\ ^1B_2$	9.96 (0.000)	12.13 (1.195)	10.32 (1.044)

and $\hat{S}^2$ expectation values computed with FCI, SF-CIS, and SF-PBE50. The ground state of methylene is the X^3B_1 state with two unpaired electrons on the carbon atom. Spin-flip expansion using the high-spin $^3B_1$ configuration contains N_S^2 Slater determinants with two electrons in the two frontier orbitals, a_1 and b_1 (singly occupied in the reference triplet), which are needed to describe the ground triplet state and three lowest singlets: 1^1A_1, 1^1B_1, and 2^1A_1. Both SF-CIS and SF-PBE50 produce virtually spin-pure states. SF-CIS energies slightly overestimate the FCI results, while the SF-PBE50 gaps are too small, which is related to the overestimation of the $M_S = 0$ triplet state energy in same-center diradicals by collinear SF-TDDFT.[34] Beyond the four lowest states, all the computed transitions produce spin-broken solutions. These results highlight the limitations of spin-flip methods in the computation of higher excited states, especially in schemes including up to single electron excitations. We note that the EOM-DEA-type of ansatz would be appropriate for treating higher excited states in diradicals.

5.3 Restoring spin completeness in SF-CIS

The deficiencies related to spin-incompleteness of the excitation operator in the CI and CC schemes can be progressively corrected by including higher excitations. Krylov and collaborators[98] corrected spin contamination in SF-CIS by explicitly adding the necessary double and triple electron excitations (with one spin-flip) to spin-complement the spin-incomplete configuration set (Fig. 11). The resulting ansatz, SC-SF-CIS, is free of spurious mixing of the states with different spin multiplicity and yields improved relative state energies, optimized geometries, and potential energy profiles along bond dissociation relative to SF-CIS. Later on, Casanova and Head-Gordon introduced the spin-flip extended single excitation CI method (SF-XCIS),[21] which expands the SC-SF-CIS space to include electronic configurations important for the description of low-lying states, that is, excitations with two paired electrons within the N_S space plus an $O \rightarrow V$ spin-conserving excitation. These configurations, which can be obtained as a subset of the $\Delta M_S = -1$ double excitation operator acting on the high-spin triplet reference, notably improve the description of molecules with large diradical character and yield better transition energies to states with large contribution of doubly excited configurations. Both methods, SC-SF-CIS and SF-XCIS, have shown to be superior to SF-CIS, with only a
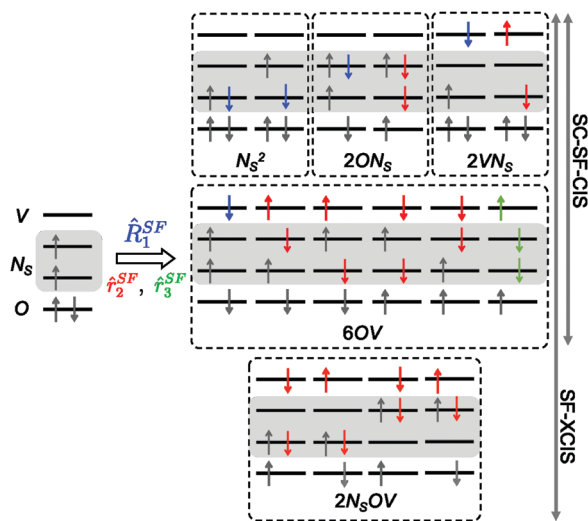
Fig. 11 Electronic configurations generated in the SC-SF-CIS and SF-XCIS methods through the full spin-flip single excitation operator (blue), a subset of the two- (red) and three-electron (green) spin-flip excitations with one spin-flip excitation applied to a high-spin triplet. N_S, O, and V: singly occupied (highlighted in grey), doubly occupied and fully virtual orbitals at the reference state. The dimension of each type of configuration subspace is indicated at the bottom.

small increase of the computational cost. The main error source in the excitation energies, as in (non-spin-flip) CIS, comes from the lack of dynamic correlation, which typically results in an over-estimation of excitation energies, especially for the one-electron singlet HOMO-to-LUMO transitions.

5.4 Spin-adapted SF-TDDFT approaches

Within TDDFT and the AA, there is no clear pathway for going beyond single excitations, which complicates the strategy towards spin-complete SF-TDDFT. Nevertheless, several promising attempts can be found in the literature. Spin contamination in SF-TDDFT can be completely eliminated through the spin-adapted version of Li and Liu based on a tensor-coupling scheme.[33,102,149] However, despite providing spin-pure states, such an approach does not ensure the degeneracy between different multiplet components, which can be only preserved with exact exchange. More recently, Zhang and Herbert have developed a spin-adapted SF-TDDFT method (SA-SF-DFT)[35] based on the *ad hoc* modification of the SC-SF-CIS matrix elements to DFT-like xc terms. The method has shown robust performance and improved accuracy.[35]

Alternatively, in order to mitigate the problems arising from spin-incompleteness in SF-TDDFT, Lee *et al.* proposed the use of mixed reference (MR) reduced density matrices built as an ensemble of high-spin ($M_S = +1$) and low-spin ($M_S = -1$) triplet densities:

$$\rho_0^{MR}(\mathbf{x}, \mathbf{x}') = \frac{1}{2}\Big(\rho_0^{M_S=-1}(\mathbf{x}, \mathbf{x}') + \rho_0^{M_S=+1}(\mathbf{x}, \mathbf{x}')\Big), \quad (13)$$

in conjunction with the definition of spinor-like open-shell orbitals.[150] As a result, the MR-SF-TDDFT response vector contains additional amplitudes that spin-complement the con-figurational space from collinear SF-TDDFT, largely reducing

spin-contamination of the computed states, especially for low-energy excitations. To completely eliminate spurious mixing between the states of different spin multiplicities, it would be necessary to include the $M_S = 0$ triplet in the definition of the MR reduced density:

$$\rho_0^{MR}(\mathbf{x}, \mathbf{x}') = \frac{1}{3}\Big(\rho_0^{M_S=-1}(\mathbf{x}, \mathbf{x}') + \rho_0^{M_S=0}(\mathbf{x}, \mathbf{x}') + \rho_0^{M_S=+1}(\mathbf{x}, \mathbf{x}')\Big). \quad (14)$$

Despite the effective elimination of spin-contamination, the effect on the state energies is small, because the coupling between configurations generated from $M_S = +1$ and $M_S = -1$ references vanishes. To circumvent this deficiency within the formalism using collinear kernels, these couplings can be added *a posteri* through configuration interaction. It is worth noticing that the increased complexity of the orbital Hessian matrix and the expanded configurational space increase the computational requirements of MR-SF-TDDFT with respect to SF-TDDFT.

6 Generalization to multiple spin-flip excitations

Spin-adapted SF-CI and SF-TDDFT schemes correct the spin incompleteness of low-order spin-flip excitation operators, but they cannot deal with low-spin states, *e.g.*, singlets or doublets, with more than three strongly correlated electrons. Thus, their application is limited to diradicals and triradicals. Treating systems with more than three unpaired electrons within the spin-flip framework requires the use of excitation operators with more spin-flips acting on references of higher spin multi-plicities, chosen in accordance with the orbital degeneracy pattern. Ideally, for n strongly correlated electrons one should use the lowest high-spin $(n + 1)$-multiplet as the reference configuration and an excitation operator with the necessary spin-flip excitations to reach the target M_S states. For example, the $M_S = 0$ states of a tetraradicaloid molecule (four correlated electrons) can be described by using an excitation operator flipping the spins of two electrons ($M_S = -2$ type) acting on a high-spin quintet reference ($M_S = +2$).

To extend the spin-flip approach beyond two or three unpaired electrons, spin-flip methods within CI and CC ansätze were extended to double spin-flip excitations.[23] The 2SF-CI and EOM-2SF-CC methods with the use of a high-spin quintet reference are able to describe tetraradicals, breaking of double bonds, or simultaneous dissociation of two single bonds. Following this strategy, one can envision tackling systems with more strongly correlated electrons by choosing higher-multiplicity reference and spin-flip operators with more spin-flips. However, such systematic increase of reference multiplicities and the number of $\alpha \rightarrow \beta$ excitations in truncated CI or CC schemes imposes some inconveniences, such as spin incompleteness of the n-spin-flip operator (much like in the single spin-flip case) and the increasing computational cost necessary to go to higher-order excitation operators.

This journal is © the Owner Societies 2020

Phys. Chem. Chem. Phys., 2020, **22**, 4326–4342 | **4337**

These limitations can be overcome by splitting the orbital space into three subsets based on the orbital occupations in the reference (high-spin) configuration: doubly occupied, singly occupied, and virtual. With this orbital classification, the spin-flip excitation operator can be expressed in terms of electronic promotions within the singly occupied space and excitation including an increasingly larger number of holes (electrons) in the doubly occupied (virtual) orbital spaces:

$$\hat{R}^{n\text{SF}} = \hat{r}_0^{n\text{SF}} + \hat{r}_h^{n\text{SF}} + \hat{r}_p^{n\text{SF}} + \hat{r}_{hp}^{n\text{SF}} + \hat{r}_{2h}^{n\text{SF}} + \hat{r}_{2p}^{n\text{SF}} + \ldots \quad (15)$$

where the $\hat{r}_0^{n\text{SF}}$ operator performs all possible spin-flip excitations within the singly occupied space (orbitals highlighted in grey in Fig. 10 and 11), while the h and p sub-indices indicate the number of electrons excited from the fully occupied orbitals (holes) and electrons promoted to the virtual space (particles). In the limit of all possible multiple hole and particle excitations, $\hat{R}^{n\text{SF}}$ reaches the FCI limit. By definition, any truncation of the rhs of eqn (15) is spin complete. This method was named restricted active space CI spin-flip (RASCI-SF or simply RAS-SF),[22,26,64,151] and the three orbital spaces are called RAS1, RAS2, and RAS3, for fully occupied, singly occupied, and unoccupied orbitals in the high-spin ROHF configuration, respectively. In fact, the SF-XCIS method can be seen as a particular case of RAS-SF that takes the high-spin triplet as the reference and uses a (single) spin-flip excitation operator including up to no more than one hole and/or one particle terms:

$$\hat{R}^{\text{SF-XCIS}} = \hat{r}_0^{\text{SF}} + \hat{r}_h^{\text{SF}} + \hat{r}_p^{\text{SF}} + \hat{r}_{hp}^{\text{SF}}. \quad (16)$$

Amongst the infinite possible truncations of eqn (15), the RAS-SF method within the hole and particle approximation, *i.e.*, $\hat{R}^{n\text{SF}} = \hat{r}_0^{n\text{SF}} + \hat{r}_h^{n\text{SF}} + \hat{r}_p^{n\text{SF}}$, provides a well-balanced ansatz with a low-computational cost (as long as the RAS2 size remains moderate). It has been successfully applied to the study of diradicals[48,152] and polyradicals,[59,153,154] the characterization of multiexcitons in multichromophoric systems,[155,156] and the modeling of singlet fission.[78,80,82,83,128] The RAS-SF approach has been further generalized to any number of orbital subspaces using the spin-flip version of the occupation-restricted multiple active space (SF-ORMAS).[30,71] Furthermore, several methodologies have sprung from RAS-SF, increasing its flexibility, *e.g.*, through the use a non-orthogonal CI strategy[24] or by means of quasidegenerate second-order perturbation theory[25] in order to alleviate the computational requirements of hole and particle contributions.

The main drawback of the hole and particle approach is the lack of effective dynamic correlation, very much like in other multi-configurational approaches, such as CASSCF. Two different solutions for recovering instantaneous electron-electron interactions have been presented: a second order perturbative correction (RAS(2)-SF)[157] and the use of short-range density functional xc kernels (RAS-SF-srDFT).[158]

An alternative strategy of extending spin-flip approach to more extensive degeneracies was proposed by Mayhall and Head-Gordon, who have demonstrated that one can construct and parameterize the Heisenberg Hamiltonian for an arbitrary number of strongly correlated electrons by performing only a single spin-flip calculation from the highest-multiplicity state.[75,76] In the case of a two-center system,[75] the exchange coupling constant is simply taken from the Landé interval rule.[159] For multiple-center systems, in which the couplings between the centers may differ, a single-spin-flip calculation is followed by additional steps in which the information of the wave functions is used to construct the Heisenberg Hamiltonian. Then the constructed Heisenberg Hamiltonian can be diagonalized, providing energies of all M_S components. Importantly, since only single spin-flip calculations are required, this approach scales linearly with the number of unpaired spins, in contrast to the factorial scaling of the full spin-flip calculation, which involves flipping the spins of $N/2$ electrons. Obviously, this scheme only works when the idealized Heisenberg physics is valid; it will break down if the unpaired electrons are strongly coupled. In these cases, a more general form of an effective Hamiltonian including non-Heisenberg terms can be used. Mayhall's approach was validated against multiple spin-flip calculations and applied to such impressive systems as a molecular magnet with 18 unpaired electrons (Cr(III) horseshoe complex), for which full spin-flip calculations are not possible.[76] When using NC-SF-TDDFT with the PBE0 functional, they obtained[76] two exchange constants, -4.38 and -4.52 cm^{-1}, in reasonable agreement with the experimental values of -5.65 and -5.89 cm^{-1}. This strategy, which can be descried as coarse-graining of electron correlation, holds much promise for tackling large strongly correlated systems.

6.1 Multiple spin-flip example: modeling singlet fission with RAS-2SF and RAS-4SF

Spin-flip methods, in particular the RAS-SF approach, have been extensively used to study the singlet fission phenomenon.[78–81,128,130–132] Singlet fission is a photophysical process taking place in organic materials in which an excited singlet state splits into two spin-coupled triplets.[82] The singlet fission efficiency depends critically on the relative state energies ($E(S_1) \approx 2E(T_1)$) and the magnitude of electronic couplings of the states involved.[130] The S_1/T_1 energy requirement is related to a moderate diradicaloid character of the singlet fission chromophore;[160] hence, the electronic structure calculations need to account for non-dynamic correlation of the two interacting diradicaloids. Moreover, because singlet fission proceeds *via* an intermediate multiexcitonic state derived by coupling two triplets into an overall singlet (often called correlated triplet-pair, ^{1}TT, or ^{1}ME), the method should be able to tackle simultaneous excitation of two electrons.

In 2016 Korovina *et al.* experimentally identified singlet fission as the main decay channel of the photoexcited covalently linked tetracene dimer, *ortho*-bis(5-ethynyltetracenyl) benzene (BET-B).[161] Singlet fission in BET-B is more efficient than in neat tetracene due to improved energetics and couplings, as revealed by electronic structure calculations.[80] The crystal structure of BET-B shows similar distances between the two intramolecular tetracene moieties and the rings of the adjacent BET-B molecules, which raises the question about potential competition between intra- and inter-molecular exciton fission. To investigate the

nature of singlet fission in BET-B, Feng *et al.* employed RAS-SF with the hole and particle approximation to analyze the electronic states of the BET-B dimer and of two interacting dimers $(BET-B)_2$, taken from the crystal structure.[80] The calculation of the BET-B molecule (two diradicaloid units) was done taking the lowest quintet state as the reference and using a double spin-flip operator, while for $(BET-B)_2$ the high-spin reference state with eight unpaired electrons was combined with a quadruple spin-flip excitation operator.

The lowest excited singlet state of BET-B corresponds to the ^1ME state, with excitonic (EX) states a few tenths of an eV above it (Fig. 12). This state ordering provides a strong energetic driving force for the triplet-pair formation upon photo-excitation to the bright state (EX_2). Then, in order to separate, the two triplets need to overcome the multi-exciton binding energy,[128] which can be evaluated as the energy difference between the singlet and quintet ME states. RAS-SF results suggest a rather strong triplet–triplet binding energy for BET-B (~ 0.4 eV), in agreement with the absence of independent triplets of BET-B in solution.[161]

The electronic state diagram of $(BET-B)_2$ is much denser than that of BET-B. The lowest excitonic states $(EX_{1,2})$ are formed as the superposition of local excitations and are largely delocalized over the four tetracene moieties. The charge-resonance states, which can be described as linear combination of ionic (or charge-transfer) configurations, are energetically close to the excitonic (*i.e.*, locally excited) states. The intra-molecular triplet-pair states (intra-^1ME) lie 0.15–0.20 eV below EX_1, with a binding energy similar to the molecular case, while the inter-^1ME states appear at higher energies (> 0.3 eV than intra-^1ME) with vanishing triplet–triplet interactions. These results and the non-zero non-adiabatic couplings between $EX_{1,2}$ and intra-$^1ME_{1,2}$ (evaluated as the norm of the one-particle transition-density matrix[128,129]) suggest that the dominant decay channel of the photo-excited system is the formation of the triplet-pair state localized on one BET-B (intramolecular singlet fission). Decoupling of the two triplets in the solid can be assisted by the formation of intermolecular ^1ME states.
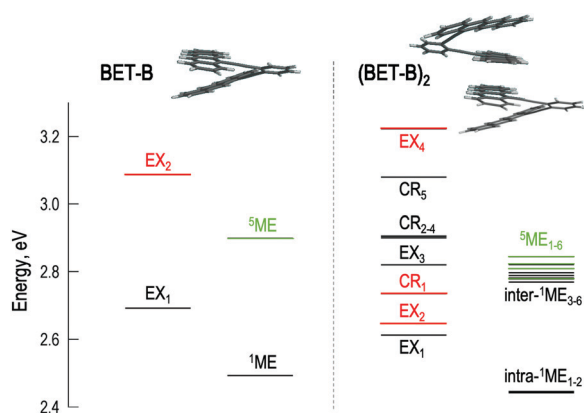

Fig. 12 Energy levels of BET–B (left) and $(BET-B)_2$ (right) computed at the RAS–SF/cc–pVDZ level. Energies were corrected by means of excited state decomposition analysis.[80] Dark, bright and quintet states marked in black, red and green, respectively. EX: excitonic state; CR: charge resonance; ME: multiexcitonic state.

7 Conclusions and perspectives

The spin-flip approach greatly expands the scope of applicability of single-reference methods. It provides a robust framework for tackling strong correlation in a fashion consistent with Theoretical Model Chemistry attributes formulated by John Pople,[11] that is, without invoking system-dependent parameterization such as active spaces or state averaging. Within wave function theory, the spin-flip idea can be combined with different levels of correlation treatment, systematically converging to the exact answer (FCI). Spin-flip also extends the applicability of Kohn–Sham DFT to multi-configurational wave functions.

Initially available only in the Q-Chem program,[162] spin-flip methods are now implemented in several other electronic structure packages. Extensive benchmarks have illustrated the reliability of the spin-flip methods and their ability to treat electronic degeneracies and interacting electronic states of different nature. Benchmark studies of state and transition properties have shown that the underlying spin-flip wave functions correctly capture the physics, resulting in accurate molecular properties. Spin-flip methods are now broadly used for describing diradicals, triradicals, single-molecule magnets, singlet fission, as well as certain types of excited state processes and non-linear optical phenomena.

Current method-development efforts include coarse-graining techniques, light-weight models for including dynamic correlation within the RAS-SF framework, spin-adaptation, and extensions aiming at computing various properties, which are important for applications. These developments are making spin-flip methods even more versatile and promise to further expand the use of spin-flip approaches.

Conflicts of interest

The authors declare the following competing financial interest(s): A. I. K. is the President and a part-owner of Q-Chem, Inc.

Acknowledgements

Notes and references

1 T. Helgaker, P. Jørgensen and J. Olsen, *Molecular electronic structure theory*, Wiley & Sons, 2000.

2 G. H. Booth, A. J. W. Thom and A. Alavi, *J. Chem. Phys.*, 2009, **131**, 054106.

3 P. G. Szalay, T. Müller, G. Gidofalvi, H. Lischka and R. Shepard, *Chem. Rev.*, 2011, **112**, 108–181.

4 N. M. Tubman, J. Lee, T. Y. Takeshita, M. Head-Gordon and K. B. Whaley, *J. Chem. Phys.*, 2016, **145**, 044112.

5 P. M. Zimmerman, *J. Chem. Phys.*, 2017, **146**, 104102.

6 J. J. Ericksen and J. Gauss, *J. Chem. Theory Comput.*, 2018, **14**, 5180–5191.

7 J. J. Ericksen and J. Gauss, *J. Chem. Theory Comput.*, 2019, **15**, 4873–4884.

8 J. Hinze, *J. Chem. Phys.*, 1973, **59**, 6424–6432.

9 B. O. Roos, P. R. Taylor and P. E. M. Siegbahn, *Chem. Phys.*, 1980, **48**, 157–173.

10 A. I. Krylov, *Acc. Chem. Res.*, 2006, **39**, 83–91.

11 J. A. Pople, *Energy, Structure and Reactivity: Proceedings of the 1972 Boulder Summer Research Conference on Theoretical Chemistry*, Wiley, New York, 1973, pp. 51–61.

12 H. Bethe, *Z. Phys.*, 1931, **71**, 205–226.

13 T. I. Shibuya and V. McKoy, *Phys. Rev. A: At., Mol., Opt. Phys.*, 1970, **2**, 2208–2218.

14 A. V. Luzanov, *Theor. Exp. Chem.*, 1982, **17**, 227–233.

15 V. Y. Krivnov, A. A. Ovchinnikov and V. O. Cheranovskii, *Synth. Met.*, 1989, **33**, 65–79.

16 A. I. Krylov, *Chem. Phys. Lett.*, 2001, **338**, 375–384.

17 A. I. Krylov, *Chem. Phys. Lett.*, 2001, **350**, 522–530.

18 A. I. Krylov and C. D. Sherrill, *J. Chem. Phys.*, 2002, **116**, 3194–3203.

19 S. V. Levchenko and A. I. Krylov, *J. Chem. Phys.*, 2004, **120**, 175–185.

20 P. U. Manohar and A. I. Krylov, *J. Chem. Phys.*, 2008, **129**, 194105.

21 D. Casanova and M. Head-Gordon, *J. Chem. Phys.*, 2008, **129**, 064104.

22 D. Casanova and M. Head-Gordon, *Phys. Chem. Chem. Phys.*, 2009, **11**, 9779–9790.

23 D. Casanova, L. V. Slipchenko, A. I. Krylov and M. Head-Gordon, *J. Chem. Phys.*, 2009, **130**, 044103.

24 N. J. Mayhall, P. R. Horn, E. J. Sundstrom and M. Head-Gordon, *Phys. Chem. Chem. Phys.*, 2014, **16**, 22694–22705.

25 N. J. Mayhall, M. Goldey and M. Head-Gordon, *J. Chem. Theory Comput.*, 2014, **10**, 589–599.

26 F. Bell, P. Zimmerman, D. Casanova, M. Goldey and M. Head-Gordon, *Phys. Chem. Chem. Phys.*, 2013, **15**, 358–366.

27 D. Ghosh, *J. Chem. Phys.*, 2013, **139**, 124116.

28 N. J. Mayhall and M. Head-Gordon, *J. Chem. Phys.*, 2014, **141**, 044112.

29 D. Lefrancois, M. Wormit and A. Dreuw, *J. Chem. Phys.*, 2015, **143**, 124107.

30 J. Mato and M. S. Gordon, *Phys. Chem. Chem. Phys.*, 2018, **20**, 2615–2626.

31 Y. Shao, M. Head-Gordon and A. I. Krylov, *J. Chem. Phys.*, 2003, **118**, 4807–4818.

32 F. Wang and T. Ziegler, *J. Chem. Phys.*, 2004, **121**, 12191.

33 Z. D. Li, W. J. Liu, Y. Zhang and B. B. Suo, *J. Chem. Phys.*, 2011, **134**, 134101.

34 Y. A. Bernard, Y. Shao and A. I. Krylov, *J. Chem. Phys.*, 2012, **136**, 204103.

35 X. Zhang and J. M. Herbert, *J. Chem. Phys.*, 2015, **143**, 234107.

36 M. de Wergifosse, C. Bannwarth and S. Grimme, *J. Phys. Chem. A*, 2019, **123**, 5815–5825.

37 A. Golubeva, A. V. Nemukhin, L. Harding, S. J. Klippenstein and A. I. Krylov, *J. Phys. Chem. A*, 2007, **111**, 13264–13271.

38 L. V. Slipchenko and A. I. Krylov, *J. Chem. Phys.*, 2002, **117**, 4694–4708.

39 V. Vanovschi, A. I. Krylov and P. G. Wenthold, *Theor. Chim. Acta*, 2008, **120**, 45–58.

40 T. Wang and A. I. Krylov, *J. Chem. Phys.*, 2005, **123**, 104304.

41 L. V. Slipchenko and A. I. Krylov, *J. Chem. Phys.*, 2003, **118**, 6874–6883.

42 R. Kishi, M. Nakano, S. Ohta, A. Takebe, M. Nate, H. Takahashi, T. Kubo, K. Kamada, K. Ohta, B. Champagne and E. Botek, *J. Chem. Theory Comput.*, 2007, **3**, 1699–1707.

43 Z. Rinkevicius and H. Årgen, *Chem. Phys. Lett.*, 2010, **491**, 132–135.

44 C. U. Ibeji and D. Ghosh, *Phys. Chem. Chem. Phys.*, 2015, **17**, 9849–9856.

45 E. Hossain, S. M. Deng, S. Gozem, A. I. Krylov, X.-B. Wang and P. G. Wenthold, *J. Am. Chem. Soc.*, 2017, **139**, 11138–11148.

46 N. Orms, D. R. Rehn, A. Dreuw and A. I. Krylov, *J. Chem. Theory Comput.*, 2017, **14**, 638–648.

47 A. Luxon, N. Orms, R. Kanters, A. I. Krylov and C. Parish, *J. Phys. Chem. A*, 2018, **122**, 420–430.

48 M. E. Sandoval-Salinas, A. Carreras and D. Casanova, *Phys. Chem. Chem. Phys.*, 2019, **21**, 9069–9076.

49 L. V. Slipchenko and A. I. Krylov, *J. Chem. Phys.*, 2003, **118**, 9614–9622.

50 L. V. Slipchenko, T. E. Munsch, P. G. Wenthold and A. I. Krylov, *Angew. Chem., Int. Ed.*, 2004, **43**, 742–745.

51 T. Wang and A. I. Krylov, *Chem. Phys. Lett.*, 2006, **425**, 196–200.

52 A. M. C. Cristian, Y. Shao and A. I. Krylov, *J. Phys. Chem. A*, 2004, **108**, 6581–6588.

53 P. U. Manohar, L. Koziol and A. I. Krylov, *J. Phys. Chem. A*, 2009, **113**, 2519–2599.

54 L. Koziol, M. Winkler, K. N. Houk, S. Venkataramani, W. Sander and A. I. Krylov, *J. Phys. Chem. A*, 2007, **111**, 5071–5080.

55 A. I. Krylov, *J. Phys. Chem. A*, 2005, **109**, 10638–10645.

56 Z. Li and W. Liu, *J. Chem. Theory Comput.*, 2016, **12**, 2517–2527.

57 F. Bell, D. Casanova and M. Head-Gordon, *J. Am. Chem. Soc.*, 2010, **132**, 11314–11322.

58 X. Lu, S. Lee, Y. Hong, H. Phan, T. Y. Gopalakrishna, T. S. Herng, T. Tanaka, M. E. Sandoval-Salinas, W. Zeng, J. Ding, D. Casanova, A. Osuka, D. Kim and J. S. Wu, *J. Am. Chem. Soc.*, 2017, **139**, 13173–13183.

59 A. Pérez-Guardiola, M. E. Sandoval-Salinas, D. Casanova, E. San-Fabián, A. J. Pérez-Jiménez and J. C. Sancho-Garca, *Phys. Chem. Chem. Phys.*, 2018, **20**, 7112–7124.

60 E. Epifanovsky and A. I. Krylov, *Mol. Phys.*, 2007, **105**, 2515–2525.

61 N. Minezawa and M. S. Gordon, *J. Phys. Chem. A*, 2009, **113**, 12749–12753.

62 N. Minezawa and M. S. Gordon, *J. Phys. Chem. A*, 2011, **115**, 7901–7911.

4340 | *Phys. Chem. Chem. Phys.*, 2020, **22**, 4326–4342

This journal is © the Owner Societies 2020

63 N. Minezawa and M. S. Gordon, *J. Chem. Phys.*, 2012, **137**, 034116.

64 D. Casanova, *J. Chem. Phys.*, 2012, **137**, 084105.

65 S. Gozem, A. I. Krylov and M. Olivucci, *J. Chem. Theory Comput.*, 2013, **9**, 284–292.

66 Y. Harabuchi, S. Maeda, T. Taketsugu, N. Minezawa and K. Morokuma, *J. Chem. Theory Comput.*, 2013, **9**, 4116–4123.

67 S. Maeda, Y. Harabuchi, T. Taketsugu and K. Morokuma, *J. Phys. Chem. A*, 2014, **118**, 12050–12058.

68 A. Nikiforov, J. A. Gamez, W. Thiel, M. Huix-Rotllant and M. Filatov, *J. Chem. Phys.*, 2014, **141**, 124122.

69 Y. Li, F. Liu, B. Wang, Q. Su, W. Wang and K. Morokuma, *J. Chem. Phys.*, 2016, **145**, 244311.

70 D. Lefrancois, D. Rehn and A. Dreuw, *J. Chem. Phys.*, 2016, **145**, 084102.

71 J. Mato and M. S. Gordon, *J. Phys. Chem. A*, 2019, **123**, 1260–1272.

72 H. R. Zhekova, M. Seth and T. Ziegler, *J. Chem. Phys.*, 2011, **135**, 184105.

73 R. Valero, F. Illas and D. G. Truhlar, *J. Chem. Theory Comput.*, 2011, **7**, 3523–3531.

74 I. Seidu, H. R. Zhekova, M. Seth and T. Ziegler, *J. Phys. Chem. A*, 2012, **116**, 2268–2277.

75 N. J. Mayhall and M. Head-Gordon, *J. Chem. Phys.*, 2014, **141**, 134111.

76 N. J. Mayhall and M. Head-Gordon, *J. Phys. Chem. Lett.*, 2015, **6**, 1982–1988.

77 N. Orms and A. I. Krylov, *Phys. Chem. Chem. Phys.*, 2018, **20**, 13127–13144.

78 D. Casanova, *J. Chem. Theory Comput.*, 2014, **10**, 324–334.

79 O. Varnavski, N. Abeyasinghe, J. Aragó, J. Serrano-Pérez, E. Ort, J. Navarrete, K. Takimiya, D. Casanova, J. Casado and I. T. Goodson, *J. Phys. Chem. Lett.*, 2015, **6**, 1375–1384.

80 X. Feng, D. Casanova and A. I. Krylov, *J. Phys. Chem. C*, 2016, **120**, 19070–19077.

81 M. H. Farag and A. I. Krylov, *J. Phys. Chem. C*, 2018, **122**, 25753–25763.

82 D. Casanova, *Chem. Rev.*, 2018, **118**, 7164–7207.

83 M. E. Sandoval-Salinas, A. Carreras, J. Casado and D. Casanova, *J. Chem. Phys.*, 2019, **150**, 204306.

84 K. D. Nanda and A. I. Krylov, *J. Chem. Phys.*, 2016, **145**, 204116.

85 K. D. Nanda and A. I. Krylov, *J. Chem. Phys.*, 2017, **146**, 224103.

86 Y. Harabuchi, K. Keipert, F. Zahariev, T. Taketsugu and M. S. Gordon, *J. Phys. Chem. A*, 2014, **118**, 11987–11998.

87 L. Yue, Y. Liu and C. Zhu, *Phys. Chem. Chem. Phys.*, 2018, **20**, 24123–24139.

88 A. V. Luzanov, *J. Struct. Chem.*, 2004, **45**, 729–739.

89 A. V. Luzanov, *Int. J. Quantum Chem.*, 2008, **108**, 671–695.

90 T. Helgaker, S. Coriani, P. Jørgensen, K. Kristensen, J. Olsen and K. Ruud, *Chem. Rev.*, 2012, **112**, 543–631.

91 R. McWeeny, *Methods of Molecular Quantum Mechanics*, Academic Press, 2nd edn, 1992.

92 D. Rowe, *Rev. Mod. Phys.*, 1968, **40**, 153–166.

93 J. Linderberg and Y. Öhrn, *Propagators in quantum chemistry*, Academic, London, 1973.

94 A. I. Krylov, *Annu. Rev. Phys. Chem.*, 2008, **59**, 433–462.

95 A. Dreuw and M. Wormit, *Wiley Interdisc. Rev.: Comput. Mol. Sci.*, 2015, **5**, 82–95.

96 J. F. Stanton and R. J. Bartlett, *J. Chem. Phys.*, 1993, **98**, 7029–7039.

97 A. I. Krylov, C. D. Sherrill and M. Head-Gordon, *J. Chem. Phys.*, 2000, **113**, 6509–6527.

98 J. S. Sears, C. D. Sherrill and A. I. Krylov, *J. Chem. Phys.*, 2003, **118**, 9084–9094.

99 P. G. Wenthold, R. R. Squires and W. C. Lineberger, *J. Am. Chem. Soc.*, 1998, **120**, 5279–5290.

100 P. G. Wenthold, J. Hu and R. R. Squires, *J. Am. Chem. Soc.*, 1996, **118**, 11865–11871.

101 J. F. Stanton and J. Gauss, *J. Chem. Phys.*, 1995, **103**, 1064–1076.

102 Z. D. Li and W. J. Liu, *J. Chem. Phys.*, 2010, **133**, 064106.

103 F. Wang and T. Ziegler, *J. Chem. Phys.*, 2005, **122**, 074109.

104 F. Wang and T. Ziegler, *Int. J. Quantum Chem.*, 2006, **106**, 2545–2550.

105 S. Yamanaka, D. Yamaki, Y. Shigeta, H. Nagao, Y. Yoshioka, N. Suzuki and K. Yamaguchi, *Int. J. Quantum Chem.*, 2000, **80**, 664–671.

106 S. Yamanaka, D. Yamaki, Y. Shigeta, H. Nagao and K. Yamaguchi, *Int. J. Quantum Chem.*, 2001, **84**, 670–676.

107 H. Eschrig and V. D. P. Servedio, *J. Comput. Chem.*, 1999, **20**, 23–30.

108 C. Van Wüllen, *J. Comput. Chem.*, 2002, **23**, 779–785.

109 F. Wang and W. Liu, *J. Chin. Chem. Soc.*, 2003, **50**, 597–606.

110 Z. Rinkevicius, O. Vahtras and H. Årgen, *J. Chem. Phys.*, 2010, **133**, 114104.

111 Z. Li and W. Liu, *J. Chem. Phys.*, 2012, **136**, 024107.

112 P. Dowd, *J. Am. Chem. Soc.*, 1966, **88**, 2587.

113 R. J. Baseman, D. W. Pratt, M. Chow and P. Dowd, *J. Am. Chem. Soc.*, 1976, **98**, 5726.

114 E. R. Davidson and W. T. Borden, *J. Am. Chem. Soc.*, 1977, **99**, 2053–2060.

115 M. Klessinger and J. Michl, *Excited States and Photochemistry of Organic Molecules*, VCH, 1995.

116 F. Bernardi, M. Olivucci and M. A. Robb, *Chem. Soc. Rev.*, 1996, **25**, 321–328.

117 C. Marian, *Wiley Interdisc. Rev.: Comput. Mol. Sci.*, 2012, **2**, 187–203.

118 *Conical intersections. Electronic structure, dynamics and spectroscopy*, ed. W. D. Domcke, D. R. Yarkony and H. Köppel, World Scientific Pbul Co Pte Ltd, 2004.

119 S. Matsika and P. Krause, *Annu. Rev. Phys. Chem.*, 2011, **62**, 621–643.

120 B. G. Levine, C. Ko, J. Quenneville and T. J. Martínez, *Mol. Phys.*, 2006, **104**, 1039–1051.

121 D. Lefrancois, D. Tuna, T. Martinez and A. Dreuw, *J. Chem. Theory Comput.*, 2017, **13**, 4436–4441.

122 X. Zhang and J. M. Herbert, *J. Chem. Phys.*, 2014, **141**, 064104.

123 J. Mato and M. S. Gordon, *Phys. Chem. Chem. Phys.*, 2020, DOI: 10.1039/C9CP05849D.

124 S. Gozem, F. Melaccio, A. Valentini, M. Filatov, M. Huix-Rotllant, N. Ferre, L. M. Frutos, C. Angeli, A. I. Krylov,

This journal is © the Owner Societies 2020

Phys. Chem. Chem. Phys., 2020, **22**, 4326–4342 | **4341**

A. A. Granovsky, R. Lindh and M. Olivucci, *J. Chem. Theory Comput.*, 2014, **10**, 3074–3084.

125 S. Gozem, F. Melaccio, R. Lindh, A. I. Krylov, A. A. Granovsky, C. Angeli and M. Olivucci, *J. Chem. Theory Comput.*, 2013, **9**, 4495–4506.

126 M. Ben-Nun and T. J. Martínez, *Chem. Phys.*, 2000, **259**, 237–248.

127 M. Barbatti, J. Paier and H. Lischka, *J. Chem. Phys.*, 2004, **121**, 11614.

128 X. Feng, A. V. Luzanov and A. I. Krylov, *J. Phys. Chem. Lett.*, 2013, **4**, 3845–3852.

129 S. Matsika, X. Feng, A. V. Luzanov and A. I. Krylov, *J. Phys. Chem. A*, 2014, **118**, 11943–11955.

130 A. B. Kolomeisky, X. Feng and A. I. Krylov, *J. Phys. Chem. C*, 2014, **118**, 5188–5195.

131 X. Feng, A. B. Kolomeisky and A. I. Krylov, *J. Phys. Chem. C*, 2014, **118**, 19608–19617.

132 X. Feng and A. I. Krylov, *Phys. Chem. Chem. Phys.*, 2016, **18**, 7751–7761.

133 P. Pokhilko, R. Shannon, D. Glowacki, H. Wang and A. I. Krylov, *J. Phys. Chem. A*, 2019, **123**, 482–491.

134 E. Epifanovsky, K. Klein, S. Stopkowicz, J. Gauss and A. I. Krylov, *J. Chem. Phys.*, 2015, **143**, 064102.

135 P. Pokhilko, E. Epifanovsky and A. I. Krylov, *J. Chem. Phys.*, 2019, **151**, 034106.

136 A. I. Krylov, *Reviews in Computational Chemistry*, J. Wiley & Sons, 2017, vol. 30, pp. 151–224.

137 P. Pokhilko, D. Izmodenov and A. I. Krylov, *J. Chem. Phys.*, DOI: 10.1063/1.5138643.

138 C. D. Sherrill, A. I. Krylov, E. F. C. Byrd and M. Head-Gordon, *J. Chem. Phys.*, 1998, **109**, 4171.

139 J. Lee and M. Head-Gordon, *J. Chem. Theory Comput.*, 2018, **14**, 5203–5219.

140 J. Lee and M. Head-Gordon, *Phys. Chem. Chem. Phys.*, 2019, **21**, 4763–4778.

141 P. G. Wenthold, *J. Org. Chem.*, 2012, **77**, 208–214.

142 E. Hossain and P. G. Wenthold, *Comput. Theor. Chem.*, 2013, **1020**, 180–186.

143 C. Sosa, J. Geertsen, G. W. Trucks and R. J. Bartlett, *Chem. Phys. Lett.*, 1989, **159**, 148–154.

144 A. Landau, K. Khistyaev, S. Dolgikh and A. I. Krylov, *J. Chem. Phys.*, 2010, **132**, 014109.

145 D. Maurice and M. Head-Gordon, *Int. J. Quantum Chem., Symp.*, 1995, **56**, 361–370.

146 P. Szalay and J. Gauss, *J. Chem. Phys.*, 2000, **112**, 4027–4036.

147 A. Ipatov, F. Cordova, L. Doriol and M. Casida, *THEOCHEM*, 2009, **914**, 60–73.

148 NIST Computational Chemistry Comparison and Benchmark Database, NIST Standard Reference Database Number 101, Release 19, April 2018, ed. Russell D. Johnson III, http://cccbdb.nist.gov, DOI: 10.18434/T47C7Z.

149 Z. Li and W. Liu, *J. Chem. Phys.*, 2011, **135**, 194106.

150 S. Lee, M. Filatov, S. Lee and C. H. Choi, *J. Chem. Phys.*, 2018, **149**, 104101.

151 D. Casanova, *J. Comput. Chem.*, 2013, **34**, 720–730.

152 M. Desroches, P. M. Burrezo, J. Boismenu-Lavoie, M. P. Álvarez, C. J. Gómez-Garca, J. M. Matxain, D. Casanova, J.-F. Morin and J. Casado, *Angew. Chem., Int. Ed.*, 2017, **56**, 16212–16217.

153 Z. Li, T. Y. Gopalakrishna, Y. Han, Y. Gu, L. Yuan, W. Zeng, D. Casanova and J. Wu, *J. Am. Chem. Soc.*, 2019, **141**, 16266–16270.

154 L. Chunchen, M. E. Sandoval-Salinas, Y. Hong, T. Y. Gopalakrishna, H. Phan, N. Aratani, T. S. Herng, J. Ding, H. Yamada, D. Kim, D. Casanova and J. Wu, *Chem*, 2018, **4**, 1586–1595.

155 A. V. Luzanov, D. Casanova, X. Feng and A. I. Krylov, *J. Chem. Phys.*, 2015, **142**, 224104.

156 D. Casanova and A. I. Krylov, *J. Chem. Phys.*, 2016, **144**, 014102.

157 D. Casanova, *J. Chem. Phys.*, 2014, **140**, 144111.

158 D. Casanova, *J. Chem. Phys.*, 2018, **148**, 124118.

159 A. Landé, *Z. Phys.*, 1923, **15**, 189–205.

160 I. Paci, J. C. Johnson, X. Chen, G. Rana, D. Popović, D. E. David, A. J. Nozik, M. A. Ratner and J. Michl, *J. Am. Chem. Soc.*, 2006, **128**, 16546–16553.

161 N. V. Korovina, S. Das, Z. Nett, X. Feng, J. Joy, A. I. Krylov, S. E. Bradforth and M. E. Thompson, *J. Am. Chem. Soc.*, 2016, **138**, 617–627.

162 A. I. Krylov and P. M. W. Gill, *Wiley Interdiscip. Rev.: Comput. Mol. Sci.*, 2013, **3**, 317–326.